ISEV

REVIEW ARTICLE

Non-Invasive imaging of extracellular vesicles: *Quo vaditis* in vivo?

Dian R. Arifin[1,2] | **Kenneth W. Witwer**[3,4] | **Jeff W. M. Bulte**[1,2,5,6,7]

[1]Russell H. Morgan Department of Radiology and Radiological Science, Division of MR Research, the Johns Hopkins University School of Medicine, Baltimore, Maryland, USA

[2]Cellular Imaging Section and Vascular Biology Program, Institute for Cell Engineering, the Johns Hopkins University School of Medicine, Baltimore, Maryland, USA

[3]Department of Molecular and Comparative Pathobiology, the Johns Hopkins University School of Medicine, Baltimore, Maryland, USA

[4]Department of Neurology, the Johns Hopkins University School of Medicine, Baltimore, Maryland, USA

[5]Department of Oncology, the Johns Hopkins University School of Medicine, Baltimore, Maryland, USA

[6]Department of Chemical & Biomolecular Engineering, the Johns Hopkins University School of Medicine, Baltimore, Maryland, USA

[7]Department of Biomedical Engineering, the Johns Hopkins University School of Medicine, Baltimore, Maryland, USA

Correspondence
Jeff W. M. Bulte, Russell H. Morgan Department of Radiology and Radiological Science, the Johns Hopkins University School of Medicine, MRB 659, 733 N. Broadway, Baltimore, MD 21205, USA.
Email: jwmbulte@mri.jhu.edu

Abstract

Extracellular vesicles (EVs) are lipid-bilayer delimited vesicles released by nearly all cell types that serve as mediators of intercellular signalling. Recent evidence has shown that EVs play a key role in many normal as well as pathological cellular processes. EVs can be exploited as disease biomarkers and also as targeted, cell-free therapeutic delivery and signalling vehicles for use in regenerative medicine and other clinical settings. Despite this potential, much remains unknown about the in vivo biodistribution and pharmacokinetic profiles of EVs after administration into living subjects. The ability to non-invasively image exogenous EVs, especially in larger animals, will allow a better understanding of their in vivo homing and retention patterns, blood and tissue half-life, and excretion pathways, all of which are needed to advance clinical diagnostic and/or therapeutic applications of EVs. We present the current state-of-the-art methods for labeling EVs with various diagnostic contrast agents and tracers and the respective imaging modalities that can be used for their in vivo visualization: magnetic resonance imaging (MRI), X-ray computed tomography (CT) imaging, magnetic particle imaging (MPI), single-photon emission computed tomography (SPECT), positron emission tomography (PET), and optical imaging (fluorescence and bioluminescence imaging). We review here the strengths and weaknesses of each of these EV imaging approaches, with special emphasis on clinical translation.

KEYWORDS
bioluminescence, CT, extracellular vesicle, imaging, MRI, PET, SPECT

1 | INTRODUCTION

Extracellular vesicles (EVs) are membranous vesicles released from nearly all cell types that function as key mediators of intercellular communication, regulating a diverse range of biological processes including cell survival, proliferation, differentiation and pathological development (Karpman et al., 2017; Kourembanas, 2015; Théry et al., 2018; Van Dongen et al., 2016; Witwer et al., 2019). Often smaller than 200 nm in diameter, EVs function in releasing unwanted cellular contents, but they also contribute to communication between cells. In addition to acting as signalling platforms, some EVs can fuse with recipient cells and transfer biologics including receptors, proteins, genetic materials (including mRNA and microRNA), and lipids, delivering a comprehensive and potentially reprogramming information package. Various subtypes of EVs have been characterized based on subcellular origin (e.g., endosomal "exosomes" and plasma membrane-derived "ectosomes" or "microvesicles"), tissue or cell source, biophysical characteristics like density and size, phenotype, and even the separation techniques used to make EV preparations. However, the existence of various competing definitions of EV subtypes should not distract from the reported benefits of EVs in the clinical setting.

Extracellular vesicles have been shown repeatedly to possess the same therapeutic capacities as their parental cells. Those derived from mesenchymal stem cells (MSCs), for example, were found to induce vascularization and to relieve ischemia (Börger et al., 2017; Giebel et al., 2017; Gong et al., 2017; Scrimgeour et al., 2019; Van Dongen et al., 2016; Wang et al., 2017). As cell-free products, EVs may offer lower immunogenicity than therapeutic cells and without the possibility of pathological transformation: they are unable to form tumours themselves. The small size of EVs may also minimize the chance of thrombosis. In addition, EVs possess several advantages associated with soluble drugs and other therapeutic molecules, such as ease of transport, convenience of administration (without the need of cell culture) and long-term storage stability (Colombo et al., 2014; Jeyaram & Jay, 2017; Phinney & Pittenger, 2017). Therefore, EVs are considered to be a safer and overall more convenient replacement of cell therapy.

Due to their unique membrane composition, EVs have complex physical and biological properties that are difficult to replicate with synthetic vesicles (Witwer & Wolfram, 2021). Their ability to cross biological barriers such as the blood brain barrier, to target and selectively internalize into specific cells, and to camouflage themselves from the recipient immune system render them an attractive choice of delivery system (Alvarez-Erviti et al., 2011; Ha et al., 2016; Lai et al., 2013; Xin et al., 2013). In diagnostic applications, endogenous EVs in biological fluids can serve as a liquid biopsy for biomarkers of disease progression (Nuzhat et al., 2017; Rajagopal & Harikumar, 2018; Sharma et al., 2017).

Related to EVs, EV mimetic-nanovesicles (NVs) are mechanically generated from cells or cellular membranes. The ease of production of these EV-like particles yielding 100 times or more those of native EVs (Jang et al., 2013; Lee et al., 2020; Wu et al., 2018) suggest strong promise. It is important to recognize that NVs may display partly different membrane topology from natively produced EVs and might also include cellular components that could be immunogenic or be perceived as danger signals. Nevertheless, these more easily produced particles may retain some or all of the beneficial properties of EVs. labeling EVs /NVs may create theranostic (i.e., combined diagnostic and therapeutic) products that can be visualized while simultaneously delivering active ingredients to target cells. In this review, we will make a distinction if NVs were used instead of EVs.

Despite the myriad demonstrated, assumed, and posited benefits of EVs or NVs, much remains unknown about the fate of these vesicles in vivo once administered (Chuo et al., 2018; Di Rocco et al., 2016; Gangadaran et al., 2017; Gao et al., 2021). The major questions to be addressed are: *Quo vaditis (where are you/they going)?* Where do these vesicles go after administration into a living subject? Do they reach the target site in a timely manner and in therapeutic quantities? What is their mechanism of action? Do EVs/NVs from different origins behave differently? Revelations about the biodistribution, pharmacokinetics, bioavailability, migration ability, local retention, toxicity, biological role/molecular mechanisms of EVs/NVs will be critical for successful translation of EV/NV-based technology from bench to bedside. We posit that successful applications of non-invasive imaging techniques will be indispensable to this progress.

1.1 | Indirect versus direct labeling of EVs/NVs

Imaging EVs or NVs is challenging due to their small size and the similarity of their molecular composition to recipient tissue. To the best of our knowledge, there are no studies on imaging label-free EVs/NVs, and only a single report on imaging endogenous EVs has been published (Hikita et al., 2020). Instead, exogenous EVs/NVs are labeled prior to administration to living subjects by routes including topical, intranasal, intravenous and intraperitoneal. Since the structure and composition of EV/NV membranes are similar to those of liposomes, labeling methods developed for liposomes can often be used to label EVs/NVs. Exogenous EV labeling approaches can be categorized as indirect (Figure 1A) and direct (Figure 1B). The same techniques can be applied for labeling NVs.

In indirect EV labeling (Figure 1A), parent cells are labeled, and these cells in turn release labeled EVs. In the case of NVs, labeled parent cells are used for NV production. Parent cells have been transduced by viral vectors carrying a reporter gene or protein (Gangadaran et al., 2017; Lai et al., 2014; Liu et al., 2020; Toribio et al., 2019). EVs isolated from these cells may bear these same labels. However, any genetic manipulation of parent cells could pose hurdles to clinical approval, since there may be concerns about malignant differentiation. Another approach utilizes nanoparticle-based labels (NPs) (Betzer et al., 2017; Dabrowska et al., 2018; Han et al., 2021; Jung et al., 2018; Kim et al., 2020; Lara et al., 2020; Lee et al., 2020; Perets et al., 2019; Tayyaba et al., 2020; Yu et al., 2019). Parent cells incubated with such NPs can take up these labels and transport them into the cytoplasm. EVs or NVs might then encapsulate them during their formation. Magnetoelectroporation has previously been used as an efficient intracellular magnetic labeling of parent cells through a temporary opening of the cell membrane (Engberink et al., 2010; Walczak et al., 2006; Walczak et al., 2005). More recently, electroporation has been used (Han et al., 2021; Hood et al., 2014; Hu et al., 2015) to introduce magnetic particles constrained to 30 nm (diameter) or smaller for labeling of smaller vesicles including exosomes or NVs (Busato et al., 2016; Dabrowska et al., 2018; Lee et al., 2020), or around 70 nm for a general mixture of larger EVs (Jc Bose et al., 2018). Perhaps magnetosonoporation (Qiu et al., 2010; Xie et al., 2010) will also find applications to produce similar magnetovesicles.

In contrast, direct labeling applies a label to EVs or NVs post-production (Figure 1B). Direct labeling is needed if manipulation of parent cells is impossible or undesirable, or if incorporation of label from parent cells is inefficient. Lipophilic probes or probes conjugated to phospholipids can be incorporated into the vesicle membrane by incubation or membrane extrusion
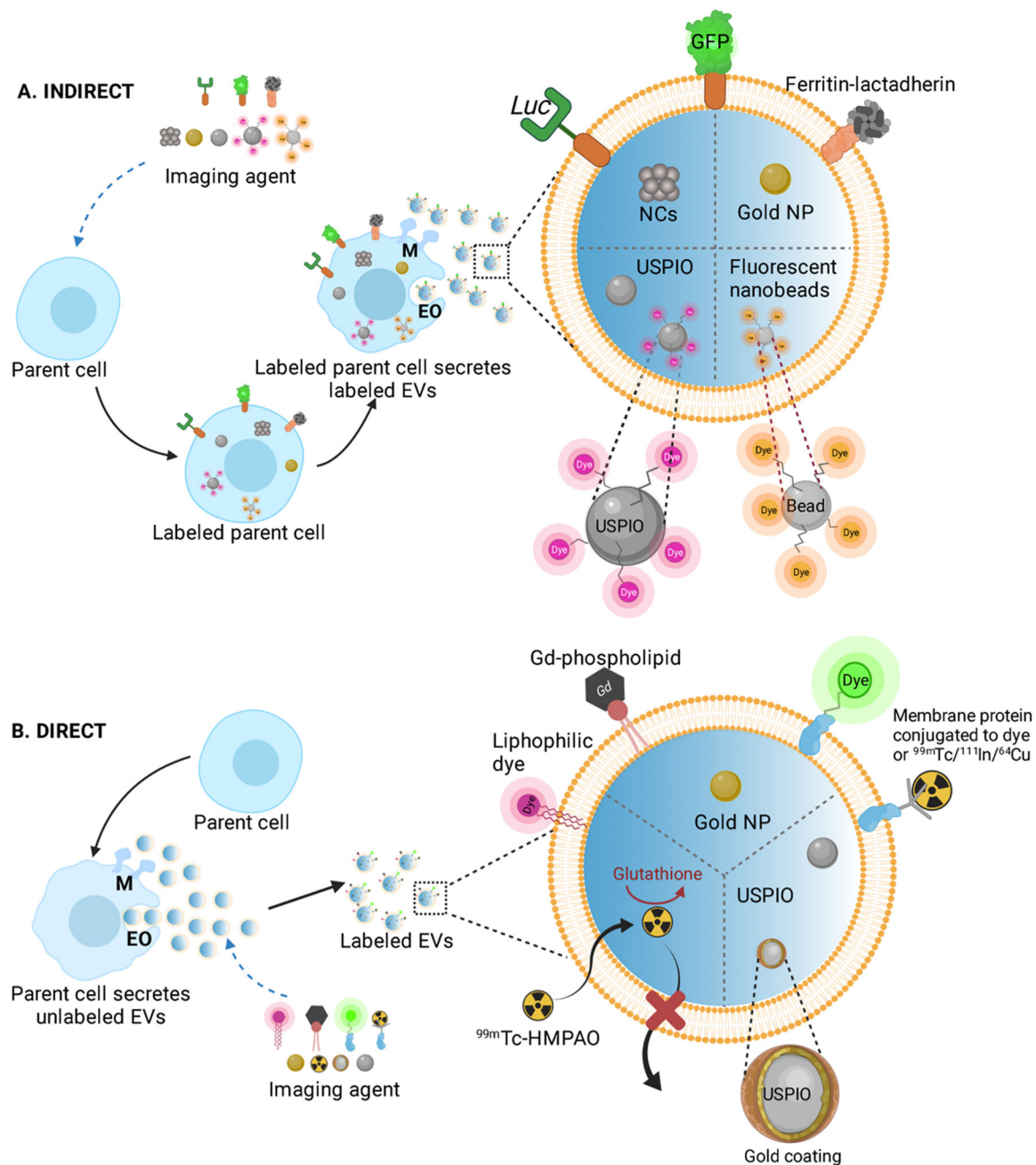
FIGURE 1 Schematic depiction of the various methods to label EVs using indirect (A) or direct labeling (B). EVs are from endosomal origin (EO) or formed by the outward budding of membranes (M). (A) Indirect methods via transduction produce EVs with membranes carrying luciferase (*Luc*) for BLI or a fluorescent protein such as GFP (Gangadaran et al., 2017; Lai et al., 2014; Toribio et al., 2019) or a ferritin heavy chain MRI reporter (Liu et al., 2020) conjugated to the trans-membrane protein lactadherin. Ultrasmall nanoparticles composed of superparamagnetic iron oxide USPIO for T_2 or T_2^*-weighted MRI (Dabrowska et al., 2018; Han et al., 2021; Kim et al., 2020; Lee et al., 2020) or MPI (Jung et al., 2018), USPIO conjugated to rhodamine for dual-mode MRI and fluorescence imaging (Dabrowska et al., 2018; Kim et al., 2020; Lee et al., 2020), gold nanoparticles (NPs) for CT (Betzer et al., 2017; Cohen et al., 2021; Lara et al., 2020; Perets et al., 2019), and silver and iron oxide nanoclusters (NCs) for fluorescence, CT and T_2-weighted MR imaging (Tayyaba et al., 2020) have also been employed. (B) EV membranes can be directly labeled by inserting agents into the membrane bilayers or by conjugating agents to the EV surface. EVs have been labeled with the lipophilic fluorescent dyes PKH26, DiI, DiD or DiR (Garofalo et al., 2019; Lassailly et al., 2010; Lehmann et al., 2016; Progatzky et al., 2013), phospholipids conjugated to Gd as T_1-weighted MRI contrast agent (Abello et al., 2019; Rayamajhi et al., 2020) or the membrane proteins of EVs conjugated to fluorescent dyes (Bakirtzi et al., 2019; Hwang et al., 2019; Shi et al., 2019; Song et al., 2020; Zhang et al., 2020), the SPECT tracers [99m]Tc (Varga et al., 2016) and [111]In (Faruqu et al., 2019; Lu et al., 2021), and the PET tracer [54]Cu (Banerjee et al., 2019; Jung et al., 2020; Shi et al., 2019). The EV core can also directly be loaded with gold nanoparticles (Cohen et al., 2021; Pan et al., 2020) or USPIOs (Han et al., 2021) or USPIOs coated with gold NPs (Jc Bose et al., 2018). SPECT radiotracers, ^{99m}Tc-hexamethylpropyleneamineoxime (HMPAO) (Hwang et al., 2015; Son et al., 2020), reacts with glutathione inside the vesicle core to trap the tracer. Cartoons were created with Biorender.com

(Abello et al., 2019; Lara et al., 2020; Lázaro-Ibáñez et al., 2021; Nishida-Aoki et al., 2020; Rayamajhi et al., 2020; Wan et al., 2020; Zhang et al., 2020), while the surface membrane proteins of EVs can be conjugated to probes (Banerjee et al., 2019; Faruqu et al., 2019; Hwang et al., 2015; Jung et al., 2020; Shi et al., 2019; Son et al., 2020; Varga et al., 2016). As in the case of magnetoelectroporation, the membranes of EVs can be temporarily opened, allowing nanoparticles to be entrapped inside the vesicle core.

Regardless of the type of label and labeling protocol, the EV/NV marker proteins, protein content, size distribution, morphology, zeta potential, bioactivity, in vitro biocompatibility and/or in vivo biodistribution were generally reported to be unaffected or insignificantly altered by labeling (Abello et al., 2019; Banerjee et al., 2019; Betzer et al., 2017; Faruqu et al., 2019; Gangadaran et al., 2017; Han et al., 2021; Hwang et al., 2015; Hwang et al., 2019; Jc Bose et al., 2018; Kim et al., 2020; Lara et al., 2020; Lee et al., 2020; Liu et al., 2020; Pan et al., 2020; Rayamajhi et al., 2020; Son et al., 2020; Song et al., 2020; Tayyaba et al., 2020; Toribio et al., 2019; Varga et al., 2016). At present, the majority of studies has only superficially characterized EVs post-labeling with only scant investigations on the effects of EV labeling at the level of proteome and nucleic acid composition (limited to EV marker, protein content and composition assays). Occasional studies have reported cytotoxicity at higher label concentration (Tayyaba et al., 2020) and an altered surface charge or size distribution of EVs (Betzer et al., 2017; Hwang et al., 2019). Labeled vesicles maintained their integrity (retention of imaging probes, size, polydispersity index, particulate form) in serum or PBS (Abello et al., 2019; Banerjee et al., 2019; Rayamajhi et al., 2020) for days, with 30 days reported to be the longest period (Rayamajhi et al., 2020). When indirect labeling methods were used, the cell viability, phenotype markers and/or the differentiation capacity of labeled parent cells were found to be similar to unlabeled cells (Lara et al., 2020; Liu et al., 2020) with only one report stating a slower proliferation rate of parent cells (Liu et al., 2020). It is needless to state that the full impact of EV labeling is still unknown, hence careful consideration must be taken in designing experiments, data analysis and interpretation.

1.2 | The many facets of tracking EVs/NVs

In elucidating the fate of EVs/NVs in vivo, there are a multitude of factors to be considered. The first is the biodistribution path that EVs/NVs take, that is, trafficking from the site of administration to the target tissue or to tissues mediating body clearance (such as the liver and kidneys). The second one is the uptake and distribution of vesicles within a recipient cell once internalized. At present, fluorescence imaging is the only technique that can capture trafficking of EVs inside a recipient mammalian cell with a limitation that this can only be done in vitro. Equally important is the ability of a specific imaging tool to provide qualitative versus quantitative assessment. Qualitative imaging offers temporal and spatial knowledge of administered EVs/NVs. Quantitative imaging, on the other hand, yields additional information on the total amount of EVs/NVs at any given time and location. The label itself can be classified as a passive or active (sometimes called "smart") label. The former enables tracking EVs/NVs without providing any other data, such as the integrity of the vesicles. Depending on the composition, passive labels may linger in tissues or in the circulation long after vesicle disintegration, potentially leading to misinterpretation of data. Meanwhile, active labels have the ability to report on both the migration pattern and integrity of EVs/NVs.

Exosomes, microvesicles, and apoptotic bodies are EV populations categorized based on their intracellular origin. However, emerging evidence suggests that even within these EV populations various subpopulations may exist, each participating in biological processes with its own contribution (Willms et al., 2018). Moreover, new research in cancer revealed that EVs secreted by cancer cells of different origins were found to be physically similar yet possessing different integrin expression patterns. This heterogeneity in cancer EVs may play a key role in metastasis organotropism (Grigoryeva et al., 2020; Hoshino et al., 2015).

Nearly all studies on tracking EVs in animal models have been performed using exogenously prepared and labeled EVs. Exogeneous EVs may have different heterogeneity and subpopulations than endogenously secreted EVs. This raises the question whether the models accurately reflect the physiological or pathological dynamics of interest. Exogenous EVs are most commonly used with EV-based therapy but the applied disease models may not represent the native properties or mechanisms of EVs for development of diagnostic tools or for basic science research. An exemplary study was done by Hikita et al. (2020), who tracked endogenously secreted EVs from subcutaneously engrafted PC3 prostate cancer cells in nude mice using a bioluminescence resonance energy transfer (BRET) system (further detailed in the optical imaging section). They reported different organ retention patterns and blood half-lives compared to administered exogeneously prepared EVs reported in the literature, but the effects of the transplant location of parental cells, route of administration and/or quantity of EVs need to be further investigated in order to draw a complete comparison.

1.3 | The current arsenal for imaging EVs/NVs

MRI, MPI, CT, SPECT, PET, and optical imaging (fluorescence, bioluminescence imaging or BLI and BRET) all have been employed for imaging EVs and NVs (Tables 1–3). MRI, CT, SPECT, and PET enable human whole body EV/NV visualization. The remaining imaging modalities can only be used for small animal whole-body imaging (Table 1). With using tracers, as in the

TABLE 1 Summary of available imaging agents, imaging utilities and clinical use.

Imaging modality	Examples of imaging agents	Basic principle	General features of imaging modality
^{1}H MRI	Gd-chelates (T_1-weighted MRI). USPIO (T_2 or T_2*-weighted MRI). FTH1 (T_2 or T_2*-weighted MRI).	By applying a strong magnetic field to align the electromagnetic moment of tissue protons (mostly from water), an MRI signal is generated by the protons' response to disrupting electromagnetic pulses, which depends on the proton's physicochemical microenvironment. A contrast agent is used to modify the local magnetic field and is detected as a change in proton signal.	Whole-body scanning. Anatomical imaging. Clinical and pre-clinical. Commonly used in the clinic for diagnosis.
X-ray/CT	Gold nanoparticles.	A CT scanner directs X-rays at an object from multiple orientations and measures X-ray intensity attenuation.	Whole-body scanning Anatomical imaging Clinical and pre-clinical Commonly used in the clinic for diagnosis and to guide interventional surgeries.
SPECT PET	^{99m}Tc, ^{111}In or ^{131}In for SPECT. ^{64}Cu for PET.	SPECT detects gamma rays emitted by radioisotopes at a series of angles using multiple gamma cameras. PET radionuclides emit positrons. Gamma rays released from collisions of electrons and positrons are detected by a PET camera at a series of angles.	Whole-body scanning. Clinical and pre-clinical. Commonly used in the clinic to analyse organ function and for diagnosis.
MPI	SPIO.	By moving the magnetic field, an MPI system creates a single magnetic field-free region where MPI tracers exhibit non-linear responses. MPI detects the tracers by moving the field-free region across an object.	Whole-body scanning. Pre-clinical
Fluorescence	Lipophilic dyes Self-quenching, cyanine-based dyes. Silver nanoclusters. Ce6 molecules.	Upon illumination with light, fluorescent dyes or proteins absorb then emit light of a longer wavelength. Different dyes or proteins emit light at different wavelengths, which are detected by a fluorescence microscope.	Whole-body scanning of small animals Ex vivo examination of harvested tissues. Pre-clinical.
BLI	Firefly/Gaussia/Renilla/NanoLuc luciferase reporter gene with luciferin or furimazine substrate.	BLI detects the photons released from an oxidation of a substrate by a luciferase enzyme.	Whole-body scanning of small animals. Pre-clinical.
BRET	teLuc (mutant of NanoLuc) fused with CyOFP1, furimazine substrate.	Photons released by the oxidation of a substrate by a luciferase enzyme is transferred to a nearby fluorescent protein through Förster resonance energy transfer. The protein in turns emits light at a specific wavelength.	Whole-body scanning of small animals. Pre-clinical.

case of MPI, SPECT and PET, absolute quantitation is possible as the tracer is detected directly corresponding to the total amount of labeled EVs/NVs. With contrast agents, as in the case of MRI, this is less straight-forward, and with optical imaging, signal is attenuated in deeper tissues with the exact depth localization is often not known. MRI and CT imaging are the only modalities that can provide an anatomical image background (Table 3). MRI produces more soft-tissue contrast than CT, as illustrated in Figure 2. The other tracer-based imaging modalities require a combination with MRI or CT to assess EVs/NVs within a meaningful anatomical context (Table 3). Most groups employed imaging tools in order to probe the biodistribution and clearance routes of EVs, and measured the accumulation of EVs in organs and tissues of interest. Only a few reported the true lowest limit of detection. Table 2 provides a summary of the lowest amount of labeled EVs retained in the smallest organs or target tissues that can be detected in vivo for each imaging modality.

1.4 | MRI

In biomedical research and clinical applications, ^{1}H or proton MRI is the most commonly used technique, taking advantage of the abundance of water in mammalian tissues. MRI contrast is determined by proton density and response to electromagnetic pulses, whereby protons in different environments produce different signals based on their "relaxation times", which in turn depend on their physicochemical microenvironment. (Para)magnetic MRI contrast agents can be used to change the local magnetic field and proton relaxation times and modify signal intensity, but one still visualizes the protons themselves and not the introduced contrast

TABLE 2 Summary of imaging resolution, sensitivity of label detection and use in EV research.

Imaging modality	Resolution	Sensitivity of detection	Extent of testing in EV research
[1]H MRI	Excellent.	Gd: 70-80 ug Gd/g tissue in vivo. USPIO: 5 μg USPIO-EVs (0.16 g iron) total or $\sim 8.76 \times 10^7$ USPIO-EVs/ml ($\sim$0.876 ng iron/ml) in vivo. FTH1: 50 μg of FTH1-EVs total in vivo.	In vitro characterization of physicochemical properties and protein markers, content, composition (Bulte, 2019; Faruqu et al., 2019; Jc Bose et al., 2018; Kim et al., 2020; Lee et al., 2020; Qiu et al., 2010; Wan et al., 2020; Yu et al., 2019). Biodistribution in mice (Bulte, 2019; Faruqu et al., 2019; Qiu et al., 2010; Wan et al., 2020; Yu et al., 2019). Magnetic guidance (Lee et al., 2020) and thermal ablation (Qiu et al., 2010) potential were tested. Tested in tumour models (Faruqu et al., 2019; Qiu et al., 2010; Wan et al., 2020) and acute kidney injury (Yu et al., 2019) models.
X-ray/CT	Excellent	10–15 μg gold/g tissue in vivo.	In vitro characterization of physicochemical properties and EV markers (Betzer et al., 2017; Engberink et al., 2010; Grigoryeva et al., 2020; Perets et al., 2019). Biodistribution in mice (Engberink et al., 2010; Grigoryeva et al., 2020; Perets et al., 2019). Tested in brain lesion (Engberink et al., 2010; Perets et al., 2019) and tumour (Grigoryeva et al., 2020) models.
SPECT PET	Poor.	[99m]Tc: 1.85–3.7 MBq/g tissue (7.25–16 μg ^{99m}Tc-EVs/g tissue) in vivo. [111]In: More than 0.035-0.07MBq/g tissue (7×10^{8} ^{111}In-EVs/g tissue) in vivo. [131]In: 648-777.8 MBq total in vivo. [64]Cu: 0.00148 MBq/g tissue in vivo.	In vitro characterization of physicochemical properties and EV markers (Hwang et al., 2015; Hwang et al., 2019; Pan et al., 2020; Son et al., 2020; Varga et al., 2016; Willms et al., 2018). Biodistribution in mice (Garofalo et al., 2019; Hwang et al., 2015; Hwang et al., 2019; Pan et al., 2020; Son et al., 2020; Varga et al., 2016; Willms et al., 2018). Circulation half-life of ^{64}Cu-EVs (Varga et al., 2016). Tested in tumour (Garofalo et al., 2019; Pan et al., 2020; Varga et al., 2016) and inflammation (Song et al., 2020) models.
MPI	Poor	5 ug iron (100 μg SPIO-EVs) in vivo.	In vitro characterization of physicochemical properties and EV markers (Lara et al., 2020). Biodistribution in mice (Lara et al., 2020). Tested in tumour models (Lara et al., 2020).
Fluorescence	Excellent for in vitro Poor for in vivo	Not determined.	In vitro characterization of physicochemical properties and EV markers (Hoshino et al., 2015; Jia et al., 2018; Jung et al., 2018). High resolution imaging in zebrafish embryos (Prince et al., 2009). Tested in tumour models (Hoshino et al., 2015; Jia et al., 2018). Ce6-induced cell apoptosis under irradiation (Hoshino et al., 2015).
BLI	Poor	3.6 μg Gaussia luc-EVs.	Biodistribution in mice (Lai et al., 2014; Toribio et al., 2019). Circulation half-life of Gaussia luc-EVs (Toribio et al., 2019).
BRET	Poor	Not determined.	Up to date, BRET-based approach is the only model for tracking endogeneouly secreted EVs (Hikita et al., 2020). Biodistribution in mice (Hikita et al., 2020). Tested in tumour models (Hikita et al., 2020).

agent. This is different from ^{19}F MRI, where the fluorine-19 atom is detected directly instead of protons. Hence, fluorinated compounds are tracers and not contrast agents, since there is no background signal due to the lack of endogenous fluorine-19 (Ruiz-Cabello et al., 2011). [1]H MRI contrast agents can be broadly categorized into T_1-weighted or "positive" contrast agents (Figure 3A, B) and T_2 or T_2*-weighted or "negative" contrast agents (Figure 3C). Positive contrast agents induced an enhancement of MRI signal (hyperintensity), whereas negative contrast agents result in a loss of MRI signal (hypointensity).

MRI is an attractive choice for whole-body tomographic imaging without the use of ionizing radiation. However, as explained above, ^{1}H MRI contrast agents are not detected directly. Artifacts due to motion, tissue haemorrhage, or the presence of air pockets may distort image interpretation and quantification analysis. MRI is therefore not the best choice for heart and gastrointestinal imaging. Moreover, MRI is not suitable for patients with pacemakers and other metal implants (Table 1–3).

TABLE 3   Summary of advantages and disadvantages of different imaging modalities.

Imaging modality	Advantages	Disadvantages
^{1}H MRI	High soft tissue contrast, providing detailed anatomical images. No radiation is involved. Long shelf-life of imaging agents.	MRI indirectly detects the protons surrounding a contrast agent. Image artifacts caused by iron (blood) and motions. MRI requires a strong magnet which necessitates non-magnetic surgical and other tools. Not suitable for patients with metal implants. The sheer size of USPIO may alter EV properties. Gd-chelates have been reported to cause nephrogenic systemic fibrosis. Lack of imaging agent quantification.
X-ray/CT	CT tracers are directly detected. Long shelf-life of imaging agents.	Patients are exposed to X-ray radiation. Poor soft-tissue resolution.
SPECT PET	Radionuclides are directly detected as 'hot Spots' without image artifacts. Incorporation into EVs is less likely to have significant effects due to the small size of label. Absolute quantification from signals.	Must be combined with MRI or CT to provide an anatomical context. Radioactive tracers are administered into patients. Short-life of probes due to radiodecay.
MPI	SPIOs are directly detected as 'hot spots' without image artifacts. No radiation is involved. Long shelf-life of imaging agents. High potential for clinical translation. Absolute quantification from signals.	Must be combined with MRI or CT to provide an anatomical context. The sheer size of SPIO may alter EV properties.
Fluorescence	Ease of labeling. Low cost. Availability of microscopes in most institutes. Incorporation into EVs is less likely to have significant effects due to the small size of label. Fluorophores are directly detected as 'hot Spots' without image artifacts.	Must be combined with MRI or CT to provide an anatomical context. Light attenuation by tissue limits deep tissue imaging. Limited to in vitro and small animals.
BLI	Differentiate intact versus non-intact (internalized) EVs in vivo (Liu et al., 2020). Signals are 'hot spots' without image artifacts. Incorporation into EVs is less likely to have significant effects due to the small size of label.	FDA is unlikely to approve administration of the xenogene and substrate into patients. Must be combined with MRI or CT to provide an anatomical context. Genetic modification of parental cells is required. Migration of substrate to *luc*-EVs are required for signal generation.
BRET	Signals are 'hot spots' without image artifacts. Incorporation into EVs is less likely to have significant effects due to the small size of label.	FDA is unlikely to approve administration of the xenogene and substrate into patients. Must be combined with MRI or CT to provide an anatomical context. Genetic modification of parental cells is required. Migration of substrate to *luc*-EVs are required for signal generation.

EVs have been labeled with paramagnetic Gd-based contrast agents (GBCA), the most commonly used MRI positive contrast agent. Gd has been conjugated to phospholipids and incorporated into macrophage-derived (Rayamajhi et al., 2020) or MSC-derived (Abello et al., 2019) EVs. EV protein markers and EV size were reported to remain unaltered post-labeling with slight changes in surface charge, size distribution and/or morphology of EVs. These changes can be expected due to the extrusion process to insert the Gd-agent into EV membranes. Intravenous (i.v.) administration of labeled (Gd and/or dye) EVs into immunodeficient mice showed an enhanced retention by target cancer cells (subcutaneous osteosarcoma in both cases), compared to the control Gd-liposomes (Rayamajhi et al., 2020), polyethylene glycol (PEG)-coated nanoparticles or the commercial GBCA Magnevist (Abello et al., 2019), and an excellent contrast enhancement in vivo, regardless of the parental cell type (Figure 3A, B). Rayamajhi et al. (2020) also reported a higher retention time of EVs in the blood vasculature compared to the single GBCA Magnevist, possibly due to EV biomimicry. in vivo and ex vivo fluorescence imaging studies in mice as well as inductively coupled plasma mass spectroscopy (ICP-MS) of harvested organs confirmed Gd-EV accumulation in the tumour, kidney, liver, lung, and heart, with an enhanced uptake by tumour. In phantom studies, clinical 3T MRI and pre-clinical 14.1T MRI detected contrast enhancement as low as 0.02–0.03 mM Gd (incorporated into EVs), showing a concentration-dependent enhancement (Abello et al., 2019; Rayamajhi et al., 2020). The lowest detection level in vivo was not determined by either group. In mouse models, tumours visualized by 3T MRI contained 0.7–0.8% ID/g tissue (70-80 μg Gd/g tissue) (Rayamajhi et al., 2020) (Figure 3B).

Ultrasmall superparamagnetic iron oxide nanoparticles (USPIOs) are the most widely used negative contrast agent to label EVs. USPIOs have been conjugated to fluorescent dyes, such as rhodamine (Dabrowska et al., 2018; Kim et al., 2020; Lee et al.,
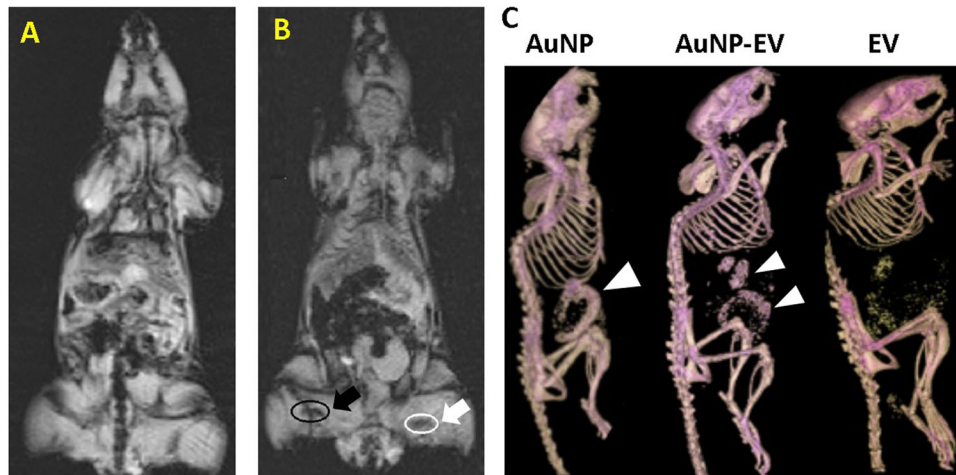
FIGURE 2 (A,B) in vivo 3T MRI of MSC-derived, ferritin heavy chain (FTH)1-labeled EVs (black circle/arrow) and unlabeled EVs (white circle/arrow) (A) pre- and (B) post-intramuscular injection into a mouse (Liu et al., 2020). Panel A and B, courtesy of Dr. X. Xin, originated from the same mouse in Liu et al. (2020). (C) in vivo mouse CT study of gold nanoparticles-labeled EVs at 24 h post-i.v. injection. AuNP = gold nanoparticles alone, AuNP-EV = labeled EVs, EV = unlabeled EVs . Arrow heads = AuNP or AuNP-EV in liver and other tissues of the reticulo-endothelial system. Panel C is adapted with permission from Lara et al. (2020).

2020), for in vitro or ex vivo histological validation or coated with gold for their use as a theranostic (combined therapeutic and diagnostic) agent (Jc Bose et al., 2018). At present, USPIO-labeling does not appear to adversely alter the protein markers, content, composition, and/or physicochemical properties of EVs or NVs (Busato et al., 2016; Han et al., 2021; Jc Bose et al., 2018; Jia et al., 2018; Lee et al., 2020; Liu et al., 2020). Interestingly, for treatment of infarcted heart, Lee et al. (2020) reported that mRNA expression, cardiac repair–related microRNAs and protein levels were significantly higher in USPIO-NVs compared to unlabeled NVs. USPIO-NVs also exhibited enhanced mechanisms of cardiac repair - higher antifibrotic, anti-inflammatory and proangiogenic effects - than unlabeled NVs in cell culture. The authors, however, did not offer any explanations for these findings (Lee et al., 2020).

Doubts nevertheless remain that incorporating nanoparticles of considerable size (20–30 nm (Lee et al., 2020)) into the core of EVs (30–200 nm) will have no or insignificant effects. Although further rigorous tests are needed to elucidate the full impact, one may surmise that such heavy nanoparticles may decrease EV mobility and modify EV circulation and biodistribution profiles. If concerns persist, commercial smaller 4–6 nm USPIOs (Busato et al., 2016; Han et al., 2021) may be used in lieu of the larger USPIOs.

USPIO-labeled EVs derived from adipose stem cells (ASCs), macrophages or human iPSCs could be detected as hypointensities in the hind limb muscle, brain and kidney in vivo in rodent models (Han et al., 2021; Jia et al., 2018; Lee et al., 2020). The reported lowest limit of detection was 3 μg (0.032 μg iron) of labeled ASC-EVs in vitro and 5 μg (0.16 g iron) in hind limb muscle at 4.7T (Busato et al., 2016). Han et al. (2021) estimated the in vivo detection limit to be ~ 8.76×10^7 labeled iPSC-EVs per ml (~0.876 ng iron per ml), assuming a 5% MRI signal change (Figure 3C).

In addition to ex vivo visualization of USPIO-labeled MSC-derived NVs in infarcted rat myocardium at pre-clinical 9.4T, this labeling strategy enabled magnetic guidance using external magnets as well as quantification of accumulated NVs (Lee et al., 2020). Magnetic steering markedly augmented retention of NVs in infarcted heart with improved cardiac function recovery. By measuring the T_2 proton relaxation rates of labeled NVs, Lee et al. (2020) estimated that magnetic guidance doubled NV retention in infarcted myocardium post-intramyocardial injection. Regardless of the promising outcome, magnetic guidance is the only clinically translatable aspect of this method since MRI of heart is fraught with motion artifacts. A secondary imaging tool will be required for EV monitoring in live recipients. In other organs and tissues, however, USPIO may dual-function as a contrast agent and magnetic guide.

The following studies are examples of suitable use of MRI to track EV migration to the brain, kidney and subcutaneous tumours in live murine models. Macrophage-derived EVs, membrane conjugated with neuropilin-1-targeted peptide to target glioma and loaded with USPIO and therapeutic curcumin, have been reported to cross the blood brain barrier (BBB) in a mouse model, with EV accumulation in the glioma visible as hypointensities (Jia et al., 2018). Compared to control native EVs, targeted EVs exhibited a higher accumulation in the glioma and stronger inhibition of tumour growth, which corresponded to the MRI data. Han et al. (2021) have created polyhistidine-coated USPIOs that enabled high labeling efficiency and simultaneous separation of magnetically labeled, human iPSC derived-EVs from free (not incorporated in EVs) USPIOs. Between 5 and 30 min after i.v. injection of these magneto-EVs, T_2*-weighted MRI visualized the renal uptake of magneto-EVs over time in a mouse model of acute kidney injury (Figure 3C). The kidneys progressively darkened due to accumulation of magneto-EVs, while an improved
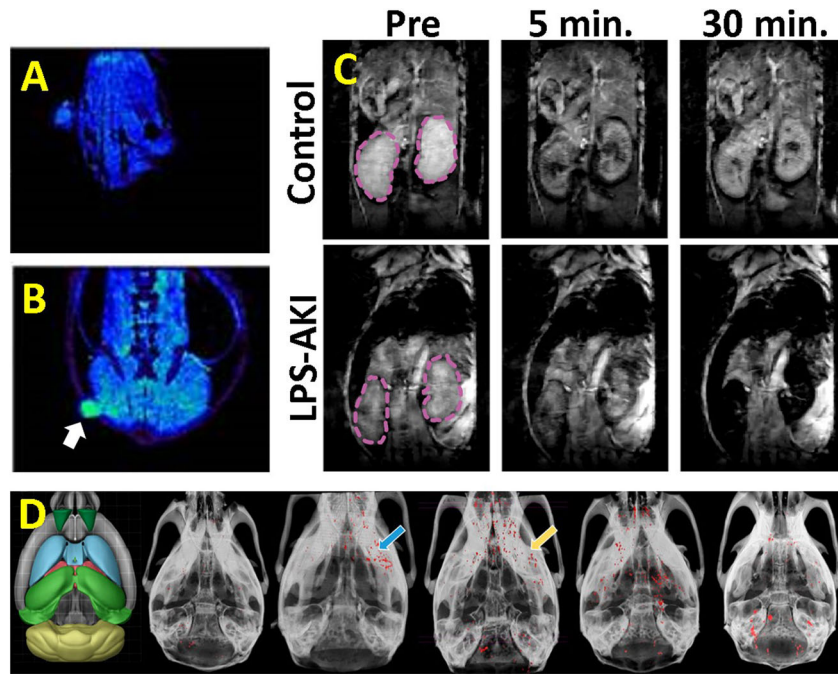
FIGURE 3 in vivo **MRI and X-ray/CT imaging**. (**A,B**) in vivo 3T MRI of MSC-derived Gd-labeled EVs in subcutaneous mouse osteosarcoma pre- (**A**) and 90 min post- (**B**) i.v. injection. Arrow = tumour with a hypointense contrast from labeled EVs (Abello et al., 2019). (**C**) in vivo T_2*-weighted 11.7T MRI of human induced-pluripotent stem cell (hiPSC)-derived USPIO-labeled EVs pre-, 5, and 30 min post-i.v. injection in a mouse model of lipopolysaccharide-induced acute kidney injury (AKI) versus control (non-injured) mice (Han et al., 2021). Kidneys are demarcated. (**D**) From left to right: Segmented mouse anatomy (dark green = olfactory bulb, blue = striatum, red = thalamus, green = hippocampus, yellow = cerebellum), and in vivo CT images of GNP-labelled, MSC derived-EVs (red) in the brain of healthy controls, stroke, Parkinson's disease, Alzheimer's disease and autism mouse models at 24 h post-nasal administration (Perets et al., 2019). Blue arrow indicates endothelin-1 injection to induce stroke; yellow arrow 6-hydroxydopamine injection to induce Parkinson's disease. Panel A and B are adapted with permission from Abello et al. (2019), panel C from Han et al. (2021), and panel D from Perets et al. (2019).

animal survival in the treated group was observed compared to the untreated group. The amount of magneto-EVs accumulated in the glioma or kidney could then be semi-quantified by analysing the changes in contrast.

Theranostic USPIOs coated with gold (GIONs) allow a combination of MRI and photothermal therapy in a single platform (Jc Bose et al., 2018). GION-loaded tumour cell-derived EVs showed high accumulation and retention in subcutaneous tumour tissue after i.v. injection, allowing specific localization of the tumour using T_2-weighted MRI. In vitro thermal ablation using a 980 nm laser of a mixture of 4T1 tumour cells and GION- EVs killed around 60% of the cells. The feasibility and efficacy of thermal ablation in animal models need to be proven in further studies. Similar to Gd-EVs, GION-EVs were mostly cleared by the liver. In all aforementioned USPIO-EV studies, MRI data were confirmed by histology and/or fluorescence imaging of rodents or harvested organs and target tissues ex vivo for the presence of fluorescently labeled NVs/EVs.

Another attractive feature of USPIO labels is their biodegradability in vivo where the iron will be recycled as haemoglobin. In summary, USPIO offers multiple additional functions in addition to imaging although the negative contrast agent is not without its shortcomings.

In a different approach, Liu et al. (2020) replaced the outer part of the trans-membrane protein lactadherin with ferritin heavy chain (FTH1), an MRI reporter. MSCs transduced with FTH1 fusion protein produced labeled EVs that in turn could be visualized by MRI in vivo after intramuscular administration into mice (Figure 2A, B). In phantoms, 5 μg/ml of FTH1-EVs showed ∼5% contrast reduction in a concentration-dependent manner, while in the muscular tissues, 50 μg of FTH1-EVs could be easily detected (Figure 2A, B). The iron content was not reported. If this method is proven to be viable, it may be a less intrusive labeling than USPIO since EVs (in this case, the membranes) are being altered with smaller sized proteins. However, early results indicated that the detection sensitivity of FTH1-EVs may be less than USPIO-EVs.

Taken together, these findings demonstrate that MRI-trackable EVs may be beneficial for early precise diagnosis and response evaluation of therapy and guided drug carriers in pre-clinical as well as clinical applications. For tumour treatment, it is not clear whether Gd-EV or USPIO-EV accumulation in the tumour is caused by their innate, targeted homing ability, longer persistence in circulation or enhanced permeability and retention (EPR) effects. Early in vitro evidence exhibited preferential uptake of Gd-EVs or GION-EVs by cancer cells versus non-cancer cells (Jc Bose et al., 2018; Rayamajhi et al., 2020), while Jia et al.'s work (Jia et al., 2018) using a glioma model showed that targeting moieties indeed enhanced BBB traversion and glioma retention.

1.5 | X-ray/CT imaging

CT imaging captures a series of X-ray projections taken from different angles to produce computer-processed tomographic pictures of a particular organ or the whole body. This modality affords ultrafast, real-time scanning, and is therefore extensively used in the clinic to guide interventional surgeries. The main drawback is exposure of patients to ionizing radiation. CT is thus not recommended for high-risk patients, such as pregnant women, or for frequently repeated imaging sessions (Table 1–3). Moreover, anatomical soft tissue images obtained by CT are not as detailed as MR images as exemplified in Figure 2.

Gold nanoparticles are the most widely used CT probe due to their excellent X-ray absorption and bioinertia. Early characterization revealed that gold-labeling did not significantly affect EV markers, size and size distribution of EVs although further tests will be required to uncover the true impacts of gold-labeling (Betzer et al., 2017; Cohen et al., 2021; Lara et al., 2020; Perets et al., 2019). Gold nanoparticles, however, are smaller (5 nm (Betzer et al., 2017; Perets et al., 2019)) than USPIO and may be less intrusive on EV core. Unlike USPIO which will eventually biodegrade, gold nanoparticles remain intact in vivo. Regardless of gold bioinertia, the mechanism of clearance from the body and the potential side effects of gold accumulation (especially in the lungs after intranasal delivery) due to repeated dosing of gold-EVs must be established.

Glucose-coated gold nanoparticles (GNPs) (Betzer et al., 2017) have been loaded into MSC-derived EVs via a GLUT-1 glucose transporter-mediated mechanism. This method was reportedly more effective than the indirect labeling method using uncoated gold (Betzer et al., 2017; Perets et al., 2019). At present, CT has been used to track GNP-EVs in the brain and tumour. Intranasal administration in mouse models of focal brain ischemia resulted in specific CT imaging of ischemic lesions as a result from accumulation of GNP-EVs in lesion sites. Betzer et al. (2017) could visualize 10–15 μg gold per g of brain tissue at 24 h post intranasal administration with distribution in the lung (majority), spleen, kidney and liver in decreasing order using a preclinical CT. About 90% of GNP-EVs in the brain accumulated in the stroke region, while in the control healthy mice, GNP-EVs did not show region-specific accumulation. Further studies demonstrated the migration and distribution patterns of GNP-EVs in mouse models of various brain pathologies, including stroke, autism, Parkinson's and Alzheimer's disease (Figure 3D). CT scans revealed the accumulation of GNP-EVs in pathologically relevant brain regions up to 96 h after delivery, while healthy controls exhibited diffuse migration and clearance by 24 h (Perets et al., 2019) (Figure 3D). Furthermore, CT imaging has been used to study the effects of EV origin on tumour targeting. CT monitoring and quantification demonstrated that i.v. delivered MSC-derived GNP-EVs had better tumour accumulation and deeper penetration into A431 subcutaneous tumour masses compared with EVs originating from A431 cells (Cohen et al., 2021).

Using a different nanoparticle coating, Lara et al. (2020) double-labeled EVs from B16F10 melanoma cells with folic acid-conjugated gold nanoparticles and the fluorescent dye DiR. CT and fluorescence imaging revealed high accumulation of i.v. injected EVs in the liver and reticulo-endothelial system (Figure 2C). The detection sensitivities of CT, however, were not adequate to visualize accumulated EVs in small tumours within the lungs (5×10^5 gold-EVs or 0.8% of injected dose) even though neutron activation analysis of tissue extracts confirmed said accumulation. This work illustrates a major challenge in EV imaging: to obtain adequate detection sensitivity for live tracking of EV retention in small target tissues. CT data were validated by histology or ex vivo fluorescence imaging of extracted tissues after administration of fluorescently labeled EVs. Furthermore, the gold amount in harvested organs and tissues were analysed by ICP-MS.

Taken together, these reports demonstrate that by employing CT imaging various groups have been able to observe the ability of EVs to home into brain lesions and tumours, allowing an in vivo assessment of origin-dependent preferential uptake of EVs by tumour cells, although the specifics of the mechanisms have not yet fully explained. Anatomical images from CT are not as detailed as MRI. However, CT can be used to image the heart and gastrointestinal tract without being compromised by motion artifacts and the presence of intestinal gas-filled pockets.

1.6 | Nuclear imaging

SPECT and PET are nuclear medicine imaging modalities commonly used to image a wide variety of therapeutics. Both detect radioactive nuclei incorporated into EVs as "hot spots", providing high sensitivity and resolution without complications from background signal artifacts, and facilitating quantification of radiolabels as tracers, as these are detected directly. The attractive feature is the use of radioactive nuclei as labels which minimally modify EVs although with a downside of radioactive exposure. SPECT directly detects gamma radiation emitted by radioisotopes at a series of angles using multiple gamma cameras, whereas PET detects pairs of gamma rays emitted indirectly by positron-emitting radiotracers. SPECT radiotracers and gamma scanning equipment are less expensive than PET. SPECT radiotracers typically have longer decay times than those of PET reagents, thus allowing a longer observation window. In addition, PET is less accessible than SPECT since a cyclotron is required to produce PET radiotracers, and an immediate transport from the production site to the imaging site is necessary due to the rapid decay of PET radioisotopes. On the other hand, rapidly decaying PET radiotracers may be preferred if less exposure to the radioactive agent is desired (Tables 1–3). Regardless of the radionuclei used, no significant changes in EV size, size distribution, morphology,
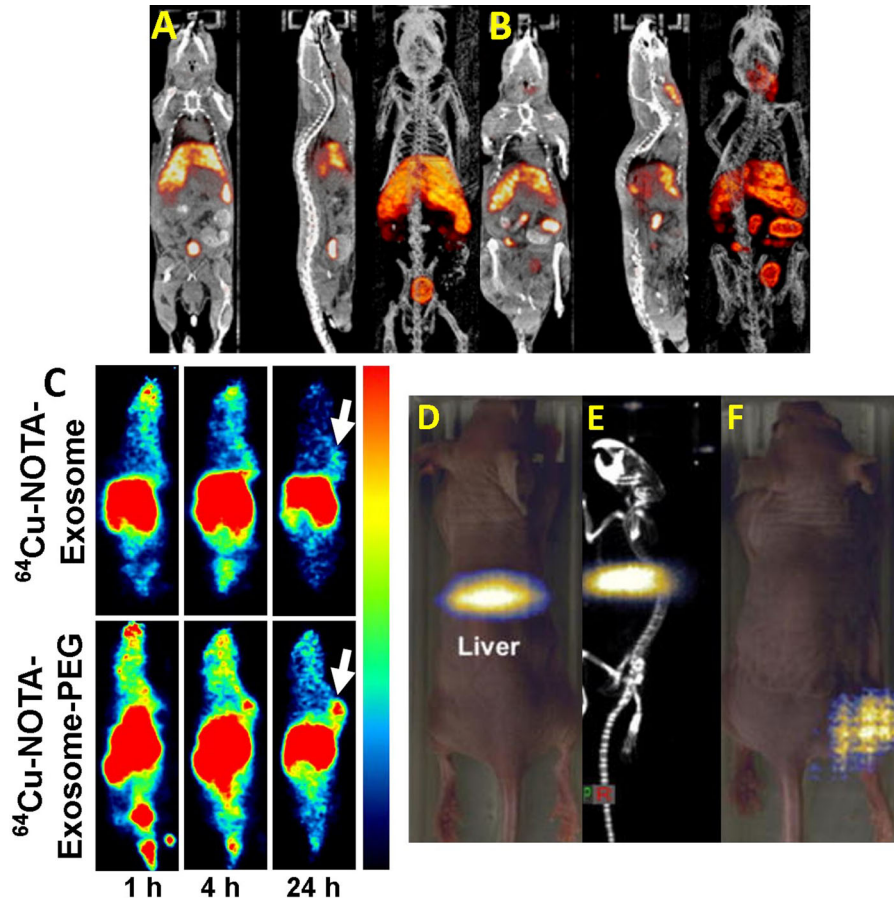
FIGURE 4 in vivo **SPECT, PET, and MPI**. (**A,B**) Overlay of SPECT/CT images of mice at (**A**) 0.5 and (**B**) 5 h post-i.v. injection of macrophage-derived, ^{99m}Tc-labeled NVs (Hwang et al., 2015). (**C**) Serial PET scans of ^{111}In-labeled, 4T1 breast cancer cell-derived exosomes. (top: non-PEGylated; bottom: PEGylated) accumulated in s.c. implanted tumours in mice (Shi et al., 2019). Arrows = tumour. Side color scale bar = 0 to 5% ID/g. (**D,F**) MPI and (**E**) MPI/micro-CT scans of SPIO-labeled, MDA-MB-231 breast cancer cell-derived exosomes accumulated in (**D,E**) liver 1 h post-IV injection and (**F**) retained in tumour after intratumoural injection (Jung et al., 2018). Panel A and B are adapted with permission from Hwang et al. (2015), panel C from Shi et al. (2019), and panel D, E and F from Jung et al. (2018).

zeta potential and EV markers post-labeling were observed (Banerjee et al., 2019; Faruqu et al., 2019; Hwang et al., 2015; Jung et al., 2020; Shi et al., 2019; Varga et al., 2016).

^{99m}Tc is the most commonly used SPECT tracer for liposome labeling and hence can be readily implemented for EV or NV tracking. In the earliest SPECT/CT studies to follow the biodistribution of NVs in vivo, Hwang et al. (2015) labeled macrophage-derived NVs using ^{99m}Tc-HMPAO. After lipophilic ^{99m}Tc-HMPAO entered the core of NVs, endogenous glutathione converted ^{99m}Tc-HMPAO to a hydrophilic form, which trapped the tracer within the core. Varga et al. (2016) labeled red blood cell (RBC)-derived EVs using a ^{99m}Tc-tricarbonyl complex that binds to the membrane proteins on the EV surface. In both studies, radiolabeled vesicles injected i.v. into mice could be captured as "hot spots", predominantly in the liver, spleen and to a minor extent also in the kidneys (Figure 4A, B). Varga et al. (2016) also quantified EV retention in the liver (67–68%), spleen (∼5%), and kidneys (∼4%). At 1 h post-delivery, the smallest visible clearance organ was arguably the spleen that trapped 1.85–3.7 MBq/g tissue (7.25–16 μg ^{99m}Tc-NVs/g tissue) in Hwang et al.'s report (Hwang et al., 2015) or a total of 0.75 MBq in Varga et al.'s report (Varga et al., 2016) (Figure 4A, B). Verification of SPECT biodistribution data was only done by the former through measurement of the radioactivity levels in extracted organs. No secondary imaging method was used for confirmation.

Other radionuclides that have been used for EV labeling include ^{111}In or ^{131}In for SPECT and ^{64}Cu for PET. Faruqu et al. (2019) and Shi et al. (2019) took advantage of the reported inherent propensity of tumour-derived EVs to be retained by tumours for delivery of anti-cancer agents. The former (Faruqu et al., 2019) labeled the membrane of B16F10 melanoma-derived EVs with ^{111}In via chelation and injected labeled EVs i.v. into melanoma-bearing immunocompetent (C57BL/6) and immunodeficient (NSG) mice. SPECT/CT images showed a minimal accumulation of signal in the tumour in both mouse groups, while EVs primarily accumulated in the liver and spleen, prompting further development of better tumour targeting strategies. Tumour tissues in C57BL/6 captured ∼0.7%ID/g tissue (0.035–0.07MBq/g tissue or 7×10^8 ^{111}In-EVs/g tissue) versus a mere ∼0.3% ID/g tissue in immunocompromised mice as measured by ex vivo gamma counting of excised organs and tissues. The tumours, however, were

not visible with SPECT, indicating that the detection limit within mice is higher than 10^8–$10^{9\ 111}$In-EVs/g tissue. The authors hypothesized that the difference in tumour accumulation values was caused by the difference in the proportion of tumour-associated macrophages within the tumour (Faruqu et al., 2019).

Shi et al. (2019) modified the surface of EVs collected from 4T1 breast cancer cells with PEG and labeled the vesicles with ^{64}Cu. PEGylation was thought to reduce premature clearance by the liver, increasing the blood half-life (~13 h) and accumulation in the tumour. Indeed, serial PET scans of 4T1 tumour-bearing mice injected with ^{64}Cu -labeled and PEGylated EVs demonstrated enhanced retention in the tumour by 3-fold at 24 h post-administration compared with their non-PEGylated counterparts (Figure 4C). The blood half-life of PEGylated EVs was obtained from region-of-interest analysis of longitudinal scans without a validation test. Shi et al. (Shi et al., 2019) hypothesized that EPR effects coupled with prolonged blood circulation increased tumour retention of PEGylated EVs. Tumours were visible with PET with an uptake of 2.7 %ID/g tissue (~1.35 μCi/g tissue or 50 MBq/g tissue) at 24 h post-i.v. injection (Figure 4C). PET biodistribution data were further validated by ex vivo gamma counting and immunohistology of harvested organs.

Meanwhile, Jung et al. (2020) conjugated ^{64}Cu-carrying 1,4,7-triazacyclononane-triacetic acid to EV membrane proteins (dual-labeled with the fluorophore Cy7) for PET imaging of the biodistribution of 4T1 cell-derived EVs. Accumulation of ^{64}Cu-EVs in brachial and axillary lymph nodes of mice could be seen with PET. PET data were confirmed by in vivo fluorescence imaging as well as ex vivo fluorescence imaging and gamma counting of extracted tissues. Smaller detectable axillary lymph nodes captured ~2%ID/g tissue or 0.00148 MBq/g tissue at 1 h after foot pad injection. Rashid et al. (2019) labeled 4T1 and AT3 tumour cell-derived EVs with ^{131}In and found their preferential accumulation at the primary tumour site and metastatic sites in the lungs using SPECT/CT. In contrast, labeled EVs from non-tumour cells showed different biodistribution profiles. ex vivo quantification by a gamma counter revealed that PET-detectable tumour contained a total of 17.5-21 μCi or 648–777.8 MBq.

The majority of SPECT or PET imaging studies is typically combined with CT. The combination of nuclear imaging with MRI has begun to be explored in order to obtain anatomical background with better soft tissue contrasts for more precise localization of labeled EVs. In the first PET/MRI study, ^{64}Cu was conjugated to the free surface thiol groups of EVs isolated from human umbilical cord blood mononuclear cells using the metal chelator 1,4,7,10-tetraazacyclododecane-1,4,7,10-tetraacetic acid (DOTA) (Banerjee et al., 2019). Serial PET/MR imaging revealed that EVs exhibited preferential accumulation in the liver, which peaked at 2 h after i.v. administration. The accumulation was the lowest in the brain with a value of 0.4–0.5% ID/g tissue (0.4–0.75 μCi/g tissue or 14.8–27.8 MBq/g tissue or 1.00-l1.75×$10^{8\ 64}$Cu-EVs/g tissue) although weak signals in the brain were still detected. The PET distribution profile, however, was not verified by other methods. In a different application for studying inflammation by gamma camera imaging, Son et al. (2020) first labeled RBC-derived NVs with ^{99m}Tc-HMPAO with ^{99m}Tc strongly binding to the alpha- and beta-globins of RBCs. White blood cells (WBCs) were subsequently labeled by incubation with ^{99m}Tc-NVs. Quantitative image analysis showed a 20-fold increase in uptake for the inflamed foot versus non-inflamed foot at 24 h after i.v. injection of ^{99m}Tc-WBC with an inflamed area uptake value of ~1%ID/g tissue or ~0.037 MBq/g tissue. However, it was hard to distinguish the signals from the inflamed region from the background. No means to validate the results were reported. The lowest limit of detection of ^{99m}Tc-labeled entities was in line with Hwang et al.'s report (1.85-3.7 MBq/g tissue) albeit SPECT was used (Hwang et al., 2015). Nuclear imaging has predominantly been used for cancer research, although other applications equally benefit from this modality. Shortcomings in the past studies include the lack of a thorough characterization of radiolabeled EVs and, in a few studies, the lack of verification of SPECT/PET data by secondary means.

1.7 | MPI

MPI is an emerging tomographic technique that directly detects SPIO nanoparticles (Bulte et al., 2015; Gleich & Weizenecker, 2005), similar to PET or SPECT, where the SPIO particles act as tracer instead of a contrast agent (Bulte, 2019). This modality has significant advantages such as sub-micromolar sensitivity (theoretically higher than ^{1}H MRI), easy image interpretation without potentially confounding background signal, and the avoidance of ionizing radiation. Unlike ^{1}H MRI, labeled entities appeared as "hot spots" on MPI (Table 1–3). To the best of our knowledge, as of today there is only a single study on MPI tracking of EVs as anti-tumour drug carriers (Jung et al., 2018). EVs were labeled with commercial VivoTrax, a 1:10 diluted formulation of Resovist, using indirect means. This commercial SPIO possesses an overall hydrodynamic diameter of 62±4 nm including the thick carboxydextran coating while the iron core itself is only 6 nm. Hence, EVs smaller than 100 nm cannot be labeled. Smaller MPI tracers are, however, currently being developed. Labeled EVs have only been superficially characterized, that is, SPIO-EVs are reported to have a similar size, distribution and EV marker make-up as their unlabeled counterparts.

As the MPI signal increases linearly with the amount of EVs in vitro, it has potential for quantitative imaging. in vivo MPI hot spot images were overlaid with anatomical images from CT (Figure 4D-F). I.v. injection of 100 μg SPIO-EVs into mice led to liver accumulation and no detectable MPI signal in the tumour (Figure 4D, E), whereas intratumoural injection induced a strong signal in the tumour (Figure 4F). Development of additional strategies for in vivo targeting/retention in tumour or tissues of interest is therefore further warranted. At the end of the observation period, harvested organs were imaged with MPI which confirmed major liver uptake unless SPIO-EVs were delivered directly to the target tissue. Validation of MPI data by a secondary

imaging method was not done. The authors (Jung et al., 2018) measured neither the limit of MPI detection nor the amount of encapsulated iron. They, however, assumed 5% w/w iron labeling, which translated to 0.125 μg iron in phantoms (2.5 μg SPIO-EVs) and 5 μg iron trapped in the tumour in vivo (100 μg SPIO-EVs, Figure 4F). The true limit of detection is expected to be lower than the tested values.

1.8 | Optical imaging

Fluorescence imaging and BLI are arguably the most widely used techniques to label EVs/NVs due to the ease of labeling, low costs, and availability of the necessary imaging equipment in the majority of research centres. Both systems allow quantification of EVs/NVs based on detected signal. Fluorescence imaging has historically been limited to the study of cell and ex vivo tissue samples, as a major drawback is the attenuation of light by tissues, and thus, this modality is not applicable for deep tissue imaging (Table 1–3). However, recent advancement in imaging technology and fluorophore chemistry permits in vivo imaging to some extent, at least in small animals (Abello et al., 2019; Garofalo et al., 2019; Lai et al., 2014). Up to this point, fluorescence imaging and BLI are considered to be research tools with limited clinical translational potential. Thus, investigations on the safety of labeling by commercial dyes, proteins and luciferase gene on EV properties and behaviour have generally not been done. A few who developed novel labels reported that labeling did not significantly modify EV markers, morphology, size and size distribution (Pan et al., 2020; Song et al., 2020; Tayyaba et al., 2020).

In early attempts at creating fluorescent EVs, lipophilic fluorescent dyes previously used to label liposomes and cells were inserted into the EV membrane. Labeling using lipophilic dyes, such as the various PKH and Di family dyes, has been reported to suffer from non-specific transfer of the dye from labeled EVs to surrounding unlabeled cells, escape of the dye from the EV membrane, formation of EV-mimicking micelles, and promiscuous labeling of contaminants of EV preparations (Garofalo et al., 2019; Lassailly et al., 2010; Lehmann et al., 2016; Progatzky et al., 2013; Pužar Dominkuš et al., 2018; Russell et al., 2019; Simonsen, 2019; Takov et al., 2017; Verweij et al., 2021). The long in vivo half-lives of these dyes worsen the problem, as the signals coming from labeled EVs are confounded by signals from transferred or released free dyes (Lai et al., 2014; Verweij et al., 2021).Therefore, the reliability and accuracy of the biodistribution data of EVs labeled using such dyes are questionable.

One way to overcome some of the aforementioned issues is to use commercially available, self-quenching, cyanine-based dyes (Collot et al., 2019; Verweij et al., 2021). The fluorogenic nature of these dyes translates to minimal fluorescent emission until they integrate into the lipid bilayer. They have recently been used to track the pharmacokinetics and biodistribution of i.v. and intranasally administered Expi293F-derived EVs in a non-human primate model (*Macaca nemestrina*) (Driedonks et al., 2021), and i.v. injected melanoma-derived EVs in zebrafish embryos (Hyenne et al., 2019). In non-human primates, fluorescence imaging was employed solely for ex vivo examination of harvested organs, as a result from the profound signal attenuation in deep tissues (Driedonks et al., 2021). In zebrafish embryos, fluorescence imaging provided high-resolution tracking of circulating tumour EVs in vivo albeit only in a mm-sized transparent organism (i.e., no signal attenuation by the skin) (Hyenne et al., 2019). As a new labeling method, parent cells (human lung adenocarcinoma A549) were engineered to produce unnatural azide groups on their surface (Song et al., 2020). Cy5 dye-conjugated dibenzylcyclooctyne was then added, linking the dye to the azide groups. After 2 days, the parent cells secreted Cy5-labeled EVs whose accumulation in the tumour sites of mouse models could be imaged for 24 h post-i.v. administration. Note that high tumour visibility in this study was due to the ectopic, subcutaneous location of the tumour and the large tumour size (larger than a mouse kidney). Naturally, this is the standard tumour model used with many other imaging modalities. However, considering the signal attenuation problems encountered with fluorescence imaging, the utility of this method in deep tissue sites has yet to be proven. Fluorophores can also be trapped inside the EV core. For direct tumour imaging, Tayyaba et al. (2020) loaded HepG2 liver cancer cells with $AgNO_3$ and $FeCl_2$, which subsequently self-assembled in situ into silver and iron oxide nanoclusters (NCs) in the presence of glutathione. Secreted EVs containing the NCs fluoresced at 579 nm in cell culture, with the potential for detection by MRI or CT. The feasibility of this new probe design in vivo is yet to be determined (Tayyaba et al., 2020). Multifunction can also be engineered into the probe as exemplified by Pan et al. (2020). EVs harvested from urine of gastric cancer patients were used to deliver Ce6 molecules to tumour sites (Pan et al., 2020). Ce6 not only exhibited fluorescence, but also induced cell apoptosis under 633 nm laser irradiation. To augment the loading efficiency, Ce6 was conjugated onto the surface of gold nanoparticles, which were then loaded into EVs via electroporation. After i.v. injection of these labeled EVs into nude mice, a deep penetration and superior retention in MGC-803 tumour sites were visualized by fluorescence imaging in vivo as well as ex vivo in extracted organs. Imaging data were confirmed using histology. This treatment resulted in enhanced apoptosis of tumour cells and a $\geq$67% increase in survival.

For BLI, EVs can be labeled with luciferase from the firefly *Photinus pyralis* (firefly luciferase, the most commonly used reporter), copepod Gaussia princeps (Gaussia luciferase) or sea pansy *Renilla reniformis* (Renilla luciferase), or alternatively with NanoLuc which is a smaller and > 150-fold brighter luciferase gene derived from the deep sea shrimp *Oplophorus gracilirostris* (England et al., 2016). However, NanoLuc-CD63 fusions have been reported to alter EV distribution, resulting in high accumulation in the lungs, demonstrating that genetic modification of EVs for tracking purposes may affect biodistribution (Lázaro-Ibáñez et al., 2021). BLI also necessitates administration of a luciferin or furimazine substrate for photon production.
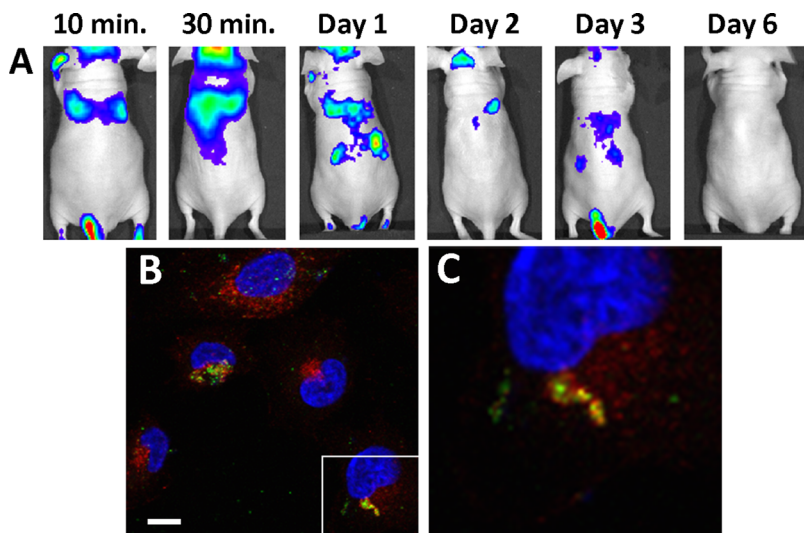
FIGURE 5 (A) in vivo serial BLI Renilla luciferase-labeled, human breast cancer MDA-MB-231 cell-derived EVs injected i.v. in a nude mouse (Gangadaran et al., 2017). (B, C) Confocal fluorescence microscopic images of dual-labeled eGFP$^+$/Renilla-labeled EVs (Toribio et al., 2019) within recipient cells. Green = EVs; blue = nucleus stained with DAPI; red = CD63, a marker of endogeneous intracellular vesicles. Scale bar = 10 μm. Panel C shows a zoomed-out inset from B. Panel A is adapted with permission from Gangadaran et al. (2017), panel B and C from Toribio et al. (2019).

Successful imaging requires penetration of the substrate to the site of imaging. These substrates would also require regulatory approval before use in patients, although there are no reports on the side effects of these substrates in animal models. BLI requires the use of nude or white mice to minimize signal attenuation by pigmented skin (Table 1–3). EVs from human thyroid cancer CAL-62 or breast cancer MDA-MB-231 cells (Gangadaran et al., 2017) and kidney HEK293T cells (Lai et al., 2014) were tagged with Renilla and Gaussia luciferase, respectively, for serial monitoring of their biodistribution and clearance (Figure 5A). This enabled a quantitative and temporal visualization of the uptake by lung, liver, spleen, and kidneys, depending on EV origin. Lai et al. (2014) and Toribio et al. (2019) developed dual reporters, with both green fluorescence and luciferase (BLI) proteins, for in vitro assessment and validation by fluorescence imaging and in vivo tracking by BLI. Spleen (46.9% retention or a total of 46.9 μg Gaussia *luc*-EVs) and liver (3.9% retention or a total of 3.6 μg Gaussia *luc*-EVs) could be clearly identified in mice (Figure 5A) with a circulation half-life of ~50 min post-i.v. injection (Lai et al., 2014). The blood half-life was not verified by other methods. Even in a small animal, the spatial resolution provided by BLI is quite poor as exemplified in Figure 5A.

Bioluminescence resonance energy transfer (BRET) is commonly used to study protein-protein interactions and has been recently applied for in vivo EV tracking. The reporter is a fused luciferase gene and fluorescent protein. Upon reaction with a substrate, luciferase acts as a donor to transfer its excited-state energy to the acceptor fluorescent protein, which in turn emits light at a specific wavelength. In an attempt to create a near physiological model (i.e., the EVs were endogeneously secreted) for probing the role of EVs in cancer metastasis, Hikita et al. (2020) used BRET to visualize and quantify the amount of EVs released by transplanted, transduced PC3 prostate cancer cells in the circulation of immunodeficient mice. The construct in this study was CD63-Antares2 with CD63 being an EV marker, while Antares2 is a NanoLuc mutant teLuc fused with fluorescent CyOFP1. Serial images of mice showed increasing amount of EVs were being secreted and dispersed over 35 days, which were confirmed by BRET of weekly drawn blood samples. Imaging and immunohistology of excised organs revealed EV accumulation in lungs, spleen, mesenteric lymph nodes and adipose tissues in genital glands and intestines. In contrast to the previous report (Takahashi et al., 2013) where injected exogenous B16-BL6 melanoma cells-derived EVs were retained in the lungs and liver, Hikita et al. mouse model showed a different EV accumulation pattern with major retention in spleen, lungs, stomach, intestines and genital glands (Hikita et al., 2020). This strategy may present a way to track and study EVs that are naturally produced by parental cells in situ, which differed in heterogeneity compared to EVs prepared for exogenous injection. However, similar to BLI, BRET was not sensitive and specific enough to non-invasively locate EV retention. In addition, cancer cell transformation by CD63-Antares2 construct does not reflect a clinical scenario.

Taken together, optical imaging is a readily available and powerful research tool for studying EVs. However, the utility is so far confined to small animal studies with poor resolution. Optical high-resolution imaging can only be performed if tissues are studied ex vivo or when using very small, transparent organisms such as zebrafish embryos.

1.9 | Imaging internalized vesicles

To date, fluorescence imaging is the only modality that has been used to track migration and distribution of EVs/NVs inside a recipient mammalian cell once they have been taken up by a said cell, albeit performed so far only on cell cultures. Toribio et al. (2019) dual-labeled EVs harvested from SUM159 breast cancer cells with eGFP (green fluorescence) and Renilla luciferase. Confocal fluorescence microscopy could visualize internalized eGFP-labeled EVs inside recipient SUM159 cells, and showed the

accumulation of EVs around the nuclei and partial colocalisation with endogenous intracellular vesicles (Figure 5B). In addition, BLI signals were detected when recipient cells pre-loaded with the BLI substrate engulfed labeled EVs. In contrast, intact EVs (not taken up by cells) remained invisible (Toribio et al., 2019). This approach may be used to monitor and identify cell uptake of EVs in a serial, non-invasive and quantitative fashion.

1.10 | In situ (in vivo) labeling of endogenous EVs

The ability to label EVs in their native state will likely lead to major discoveries, which will help us to better understand the molecular mechanisms of EVs. To the best of our knowledge, the only study that closely achieved this feat was performed by Hikita et al. (2020), where CD63-Antares2-labelled PC3 cancer cells were implanted into immunodeficient mice. EVs secreted by said cells were tracked with BRET albeit with very poor spatial specificity, as described above. At present, we are not aware of any published work on the development of exogeneous probes that can target and label specific endogenous EVs in vivo.

1.11 | Future perspectives on EV/NV imaging

In pre-clinical studies, the majority of EV/NV tracking studies has been performed using immunodeficient animal models, and therefore warrants further investigations using immunocompetent models that more closely mimic clinical cases. In the field of cancer research, it must be realized that commonly employed tumour models are ectopic and subcutaneous, large, in a known location and within an immunodeficient environment. Selection of imaging modality and probe, and imaging protocol optimization are key for sensitive and accurate detection of labeled EVs/NVs in small and/or scattered tumours in unknown deep tissue locations. This is also true for other small target tissues. Methods to address these challenges include development of new labeling protocols or probe designs to improve detection sensitivity as well as strategies to increase EV retention in tissues of interest. The mechanisms that drive selective EV/NV accumulation in a tumour, injury lesion or other specific site have not yet been fully understood although the phenomenon of tissue homing selectivity has been repeatedly observed by various groups. Imaging is a powerful tool that can help to shed more light on these EV "homing" mechanisms, and has demonstrated that incorporation of targeting moieties (Jia et al., 2018), parental lineage of EVs/NVs (Cohen et al., 2021) or strategies to prolong systemic circulation of EVs/NVs (Shi et al., 2019) in rodent models can influence EV/NV retention in target tissues.

Combination of imaging with drug delivery applications has shown potential for image-guided, EV-based drug carriers. Based on rodent studies, off-target EV/NV accumulation (with most EVs/NVs having been administered off-target) may harm the clearance organs with the liver, spleen and kidneys being at most risk. For example, Gd-based MRI agents have been associated with nephrogenic systemic fibrosis in patients with kidney dysfunction (Prince et al., 2009; Weinreb & Abu-Alfa, 2009), and therefore its use for injured kidney imaging ought to be avoided. To circumvent the clearance organs or minimize uptake, various groups have investigated administration routes other than i.v., and enhanced or incorporated targeting moeities into EVs/NVs to reduce off-target retention.

EV/NV heterogeneity is an emerging theme with its own analytical challenges. At present, EVs/NVs are exogeneously labeled in bulk prior to administration into animals without the ability to remotely identify, distinguish and independently detect one EV/NV subtype from the others within the population. (Immuno)fluorescence imaging, which is limited to in vitro studies and superficial tissue locations in small animals, is the only robust method to achieve this. Potential solutions include label-free techniques to image unique molecules native to EVs as well as methods to multi-label different EVs/NVs that enable clinically relevant imaging of different EVs/NVs at the same time. Nevertheless, it is a long road for the development of said methods as the profoundly low detection sensitivity due to the EV/NV nano-size will be a major hurdle. Current labels and labeling/imaging protocols are able to provide anatomical and cellular-level distribution of EVs or NVs in animal models and in cell cultures. The ability to image EVs or NVs at a subcellular level will drastically advance our understanding of these vesicles' molecular mechanism. Subcellular studies, however, are fraught with label promiscuity and necessitate further refinement. Up to this point, EVs/NVs have been passively tracked, that is, the only information gathered has been the spatial and temporal distribution of these vesicles in vivo. So-called 'smart' or functional labels that can also remotely report on the functions of EVs/NVs may have a profound impact to better understand EV/NV mechanisms. Such a feature has already been demonstrated using BLI where internalization of *luc*-EVs by recipient cells in mice could be detected as signal loss (Toribio et al., 2019).

From a clinical perspective, translation of EV/NV imaging techniques from bench to bedside demands a different set of investigations. In order to gauge the clinical feasibility of a particular technique, the safety and shelf-life of EV/NV labels or labeled vesicles, the clinical feasibility of the products (including the costs of GMP production and the likelihood of FDA approval), and the specific logistics of the clinical utilization of EV/NV imaging (i.e., mode and dose of administration, timing of image follow-up, availability of imaging equipment across hospitals) need to be established. It is imperative to understand that not all of imaging modalities are suitable for clinical use. MRI, CT, SPECT and PET are all clinical imaging modalities. MPI, however, is in its infancy, demanding extensive research and development efforts to bring the hardware to the clinical market and to

generate efficient SPIO tracers with FDA approval and at a clinically required scale. Optical imaging techniques have been mostly confined to pre-clinical research involving cells, tissues and small animals with their clinical translational potential remains to be limited. Another modality, ultrasonography or ultrasound (US) imaging, has not been explored yet for EV/NV imaging. While US imaging is fast, safe, relatively inexpensive, and commonly used in all hospitals and out-patient centres, a micrometre-sized bubble US contrast agent does not fit inside either EVs or NVs.

Although a few clinical trials of EV-based therapies have been performed (Dai et al., 2008; Escudier et al., 2005), the biodistribution of EVs in the patient is still unknown. These trials instead relied on downstream evaluation tools, such as bloodwork, and the final outcomes of therapy. As yet, there are no reported clinical trials on NVs. Temporospatial monitoring of EVs/NVs would provide complete information on the in vivo behaviour of EVs/NVs from the initial point of administration until the end of treatment and facilitate assessment, refinement, and approval of EV/NV therapies. Needless to say, imaging of these vesicles may accelerate the clinical translation of EV/NV-based therapies through improving the accuracy and precision of EV/NV-based medicine. In addition, the use of imaging is not limited to EV/NV-based medicine and diagnosis. For efforts to improve protocols and methods of EV/NV purification and manipulation, imaging can be used to evaluate EV/NV performance in their native environment, which in turn can be used as feedbacks to further improve EV/NV preparation protocols.

ORCID

Dian R. Arifin https://orcid.org/0000-0003-0026-819X
Kenneth W. Witwer https://orcid.org/0000-0003-1664-4233
Jeff W. M. Bulte https://orcid.org/0000-0003-1202-1610

REFERENCES

Abello, J., Nguyen, T. D. T., Marasini, R., Aryal, S., & Weiss, M. L. (2019). Biodistribution of gadolinium- and near infrared-labeled human umbilical cord mesenchymal stromal cell-derived exosomes in tumor bearing mice. *Theranostics*, *9*(8), 2325–2345.[CrossRef] PMID: 31149047.

Alvarez-Erviti, L., Seow, Y., Yin, H., Betts, C., Lakhal, S., & Wood, M. J. A. (2011). Delivery of siRNA to the mouse brain by systemic injection of targeted exosomes. *Nature Biotechnology*, *29*(4), 341–345. [CrossRef] PMID: 21423189.

Bakirtzi, K., Man Law, I. K., Fang, K., Iliopoulos, D., & Pothoulakis, C. (2019). MiR-21 in Substance P-induced exosomes promotes cell proliferation and migration in human colonic epithelial cells. *American Journal of Physiology Gastrointestinal and Liver Physiology*, *317*(6), G802–G810. [CrossRef] PMID: 31545921.

Banerjee, A., Alves, V., Rondão, T., Sereno, J., Neves, Â., Lino, M., Ribeiro, A., Abrunhosa, A. J., & Ferreira, L. S. (2019). A positron-emission tomography (PET)/magnetic resonance imaging (MRI) platform to track in vivo small extracellular vesicles. *Nanoscale*, *11*(28), 13243–13248. [CrossRef] PMID: 31290510.

Betzer, O., Perets, N., Angel, A., Motiei, M., Sadan, T., Yadid, G., Offen, D., & Popovtzer, R. (2017). in vivo neuroimaging of exosomes using gold nanoparticles. *ACS Nano*, *11*(11), 10883–10893. [CrossRef] PMID: 28960957.

Börger, V., Bremer, M., Ferrer-Tur, R., Gockeln, L., Stambouli, O., Becic, A., & Giebel, B. (2017). Mesenchymal stem/stromal cell-derived extracellular vesicles and their potential as novel immunomodulatory therapeutic agents. *International Journal of Molecular Sciences*, *18*(7), 1-19. [CrossRef].

Bulte, J. W. M. (2019). Superparamagnetic iron oxides as MPI tracers: A primer and review of early applications. *Advanced Drug Delivery Reviews*, *138*, 293–301. [CrossRef] PMID: 30552918.

Bulte, J. W. M., Walczak, P., Janowski, M., Krishnan, K. M., Arami, H., Halkola, A., Gleich, B., & Rahmer, J. (2015). Quantitative "Hot Spot" Imaging of Transplanted Stem Cells using Superparamagnetic Tracers and Magnetic Particle Imaging (MPI). *Tomography*, *1*(2), 91–97. [CrossRef] PMID: 26740972.

Busato, A., Bonafede, R., Bontempi, P., Scambi, I., Schiaffino, L., Benati, D., Malatesta, M., Sbarbati, A., Marzola, P., & Mariotti, R. (2016). Magnetic resonance imaging of ultrasmall superparamagnetic iron oxide-labeled exosomes from stem cells: A new method to obtain labeled exosomes. *International Journal of Nanomedicine*, *11*, 2481–2490. PMID: 27330291.

Chuo, S. T.-Y., Chien, J. C.-. Y., & Lai, C. P.-. K. (2018). Imaging extracellular vesicles: Current and emerging methods. *Journal of Biomedical Science*, *25*(1), 91.[CrossRef] PMID: 30580764.

Cohen, O., Betzer, O., Elmaliach-Pnini, N., Motiei, M., Sadan, T., Cohen-Berkman, M., Dagan, O., Popovtzer, A., Yosepovich, A., Barhom, H., Michaeli, S., & Popovtzer, R. (2021). 'Golden' exosomes as delivery vehicles to target tumors and overcome intratumoral barriers: in vivo tracking in a model for head and neck cancer. *Biomaterials Science*, *9*(6), 2103–2114. [CrossRef] PMID: 33475633.

Collot, M., Ashokkumar, P., Anton, H., Boutant, E., Faklaris, O., Galli, T., Mély, Y., Danglot, L., & Klymchenko, A. S. (2019). MemBright: A family of fluorescent membrane probes for advanced cellular imaging and neuroscience. *Cell Chemical Biology*, *26*(4), 600–614 e7. [CrossRef] PMID: 30745238.

Colombo, M., Raposo, G., & Théry, C. (2014). Biogenesis, secretion, and intercellular interactions of exosomes and other extracellular vesicles. *Annual Review of Cell and Developmental Biology*, *30*, 255–289. [CrossRef] PMID: 25288114.

Dabrowska, S., Del Fattore, A., Karnas, E., Frontczak-Baniewicz, M., Kozlowska, H., Muraca, M., Janowski, M., & Lukomska, B. (2018). Imaging of extracellular vesicles derived from human bone marrow mesenchymal stem cells using fluorescent and magnetic labels. *International Journal of Nanomedicine*, *13*, 1653–1664. [CrossRef] PMID: 29593411.

Dai, S., Wei, D., Wu, Z., Zhou, X., Wei, X., Huang, H., & Li, G. (2008). Phase I clinical trial of autologous ascites-derived exosomes combined with GM-CSF for colorectal cancer. *Molecular Therapy*, *16*(4), 782–790. [CrossRef] PMID: 18362931.

Di Rocco, G., Baldari, S., & Toietta, G. (2016). Towards therapeutic delivery of extracellular vesicles: strategies for in vivo tracking and biodistribution analysis. *Stem Cells International*, *2016*, 5029619.[CrossRef] PMID: 27994623.

Driedonks, T., Jiang, L., Carlson, B., Han, Z., Liu, G., Queen, S. E., et al., & Witwer, K. W. (2021). Pharmacokinetics and biodistribution of extracellular vesicles administered intravenously and intranasally to Macaca nemestrina. *Biorxiv. Preprint*, https://doi.org/10.1101/2021.07.28.454192 bioRxiv

Engberink, R. D. O., Van Der Pol, S. M. A., Walczak, P., Van Der Toorn, A., Viergever, M. A., Dijkstra, C. D., Bulte, J. W. M., De Vries, H. E., & Blezer, E. L. A. (2010). Magnetic resonance imaging of monocytes labeled with ultrasmall superparamagnetic particles of iron oxide using magnetoelectroporation in an animal model of multiple sclerosis. *Molecular Imaging*, *9*(5), 268–277. [CrossRef] PMID: 20868627.

England, C. G., Ehlerding, E. B., & Cai, W. (2016). NanoLuc: A small luciferase is brightening up the field of bioluminescence. *Bioconjugate Chemistry*, *27*(5), 1175–1187. [CrossRef] PMID: 27045664.

Escudier, B., Dorval, T., Chaput, N., André, F., Caby, M.-P., Novault, S., Flament, C., Leboulaire, C., Borg, C., Amigorena, S., Boccaccio, C., Bonnerot, C., Dhellin, O., Movassagh, M., Piperno, S., Robert, C., Serra, V., Valente, N., Le Pecq, J.-B., … Zitvogel, L. (2005). Vaccination of metastatic melanoma patients with autologous dendritic cell (DC) derived-exosomes: Results of thefirst phase I clinical trial. *Journal of Translational Medicine*, *3*(1), 1–13.[CrossRef] PMID: 15740633.

Faruqu, F. N., Wang, J. T.-. W., Xu, L., Mcnickle, L., Chong, E. M.-. Y., Walters, A., Gurney, M., Clayton, A., Smyth, L. A., Hider, R., Sosabowski, J., & Al-Jamal, K. T. (2019). Membrane radiolabelling of exosomes for comparative biodistribution analysis in immunocompetent and immunodeficient mice - A novel and universal approach. *Theranostics*, *9*(6), 1666–1682. [CrossRef] PMID: 31037130.

Gangadaran, P., Hong, C. M., & Ahn, B.-C. (2017). Current perspectives on in vivo noninvasive tracking of extracellular vesicles with molecular imaging. *BioMed research international*, *2017*, 9158319, 1–11. [CrossRef] PMID: 28246609.

Gangadaran, P., Li, X. J., Lee, H. W., Oh, J. M., Kalimuthu, S., Rajendran, R. L., Son, S. H., Baek, S. H., Singh, T. D., Zhu, L., Jeong, S. Y., Lee, S.-W., Lee, J., & Ahn, B.-C. (2017). A new bioluminescent reporter system to study the biodistribution of systematically injected tumor-derived bioluminescent extracellular vesicles in mice. *Oncotarget*, *8*(66), 109894–109914. [CrossRef] PMID: 29299117.

Gao, Y., Chu, C., Jablonska, A., Bulte, J. W. M., Walczak, P., & Janowski, M. (2021). Imaging as a tool to accelerate the translation of extracellular vesicle-based therapies for central nervous system diseases. *Wiley Interdisciplinary Reviews: Nanomedicine and Nanobiotechnology*, *13*(3), e1688.[CrossRef] PMID: 33336512.

Garofalo, M., Villa, A., Rizzi, N., Kuryk, L., Rinner, B., Cerullo, V., Yliperttula, M., Mazzaferro, V., & Ciana, P. (2019). Extracellular vesicles enhance the targeted delivery of immunogenic oncolytic adenovirus and paclitaxel in immunocompetent mice. *Journal of Controlled Release : Official Journal of the Controlled Release Society*, *294*, 165–175. [CrossRef] PMID: 30557650.

Giebel, B., Kordelas, L., & Börger, V. (2017). Clinical potential of mesenchymal stem/stromal cell-derived extracellular vesicles. *Stem Cell Investigator*, *4*, 84.[CrossRef] PMID: 29167805.

Gleich, B., & Weizenecker, J. (2005). Tomographic imaging using the nonlinear response of magnetic particles. *Nature*, *435*(7046), 1214–1217. [CrossRef] PMID: 15988521.

Gong, M., Yu, B., Wang, J., Wang, Y., Liu, M., Paul, C., Millard, R. W., Xiao, D.-S., Ashraf, M., & Xu, M. (2017). Mesenchymal stem cells release exosomes that transfer miRNAs to endothelial cells and promote angiogenesis. *Oncotarget*, *8*(28), 45200–45212. [CrossRef] PMID: 28423355.

Grigoryeva, E. S., Savelieva, O. E., Popova, N. O., Cherdyntseva, N. V., & Perelmuter, V. M. (2020). Do tumor exosome integrins alone determine organotropic metastasis? *Molecular Biology Reports*, *47*(10), 8145–8157. [CrossRef] PMID: 32929649.

Ha, D., Yang, N., & Nadithe, V. (2016). Exosomes as therapeutic drug carriers and delivery vehicles across biological membranes: Current perspectives and future challenges. *Acta Pharmaceutica Sinica. B*, *6*(4), 287–296. [CrossRef] PMID: 27471669.

Han, Z., Liu, S., Pei, Y., Ding, Z., Li, Y., Wang, X., Zhan, D., Xia, S., Driedonks, T., Witwer, K. W., Weiss, R. G., Zijl, P. C. M., Bulte, J. W. M., Cheng, L., & Liu, G. (2021). Highly efficient magnetic labeling allows MRI tracking of the homing of stem cell-derived extracellular vesicles following systemic delivery. *Journal of Extracellular Vesicles*, *10*(3), e12054.[CrossRef] PMID: 33489014.

Hikita, T., Miyata, M., Watanabe, R., & Oneyama, C. (2020). in vivo imaging of long-term accumulation of cancer-derived exosomes using a BRET-based reporter. *Science Reports*, *10*(1), 16616.[CrossRef] PMID: 33024173.

Hood, J. L., Scott, M. J., & Wickline, S. A. (2014). Maximizing exosome colloidal stability following electroporation. *Analytical Biochemistry*, *448*, 41–49. [CrossRef] PMID: 24333249.

Hoshino, A., Costa-Silva, B., Shen, T.-L., Rodrigues, G., Hashimoto, A., Tesic Mark, M., Molina, H., Kohsaka, S., Di Giannatale, A., Ceder, S., Singh, S., Williams, C., Soplop, N., Uryu, K., Pharmer, L., King, T., Bojmar, L., Davies, A. E., Ararso, Y., … Lyden, D. (2015). Tumour exosome integrins determine organotropic metastasis. *Nature*, *527*(7578), 329–335. [CrossRef] PMID: 26524530.

Hu, L., Wickline, S. A., & Hood, J. L. (2015). Magnetic resonance imaging of melanoma exosomes in lymph nodes. *Magnetic Resonance in Medicine*, *74*(1), 266–271. [CrossRef] PMID: 25052384.

Hwang, D. W., Jo, M. J., Lee, J. H., Kang, H., Bao, K., Hu, S., Baek, Y., & Moon, H. G. (2019). Chemical modulation of bioengineered exosomes for tissue-specific biodistribution. *Advances in Therapy (Weinh)*, *2*(11), 1-18. PMID: 32318623.

Hwang, D. W., Choi, H., Jang, S. C., Yoo, M. Y., Park, J. Y., Choi, N. E., Oh, H. J., Ha, S., Lee, Y.-S., Jeong, J. M., Gho, Y. S., & Lee, D. S. (2015). Noninvasive imaging of radiolabeled exosome-mimetic nanovesicle using (99m)Tc-HMPAO. *Science Reports*, *5*, 15636.[CrossRef] PMID: 26497063.

Hyenne, V., Ghoroghi, S., Collot, M., Bons, J., Follain, G., Harlepp, S., Mary, B., Bauer, J., Mercier, L., Busnelli, I., Lefebvre, O., Fekonja, N., Garcia-Leon, M. J., Machado, P., Delalande, F., López, A. A., Silva, S. G., Verweij, F. J., Van Niel, G., … Goetz, J. G. (2019). Studying the fate of tumor extracellular vesicles at high spatiotemporal resolution using the zebrafish embryo. *Developmental Cell*, *48*(4), 554–572e7. [CrossRef] PMID: 30745140.

Jang, S. C., Kim, O. Y., Yoon, C. M., Choi, D.-S., Roh, T.-Y., Park, J., Nilsson, J., Lötvall, J., Kim, Y.-K., & Gho, Y. S. (2013). Bioinspired exosome-mimetic nanovesicles for targeted delivery of chemotherapeutics to malignant tumors. *ACS Nano*, *7*(9), 7698–7710. [CrossRef] PMID: 24004438.

Jc Bose, R., Uday Kumar, S., Zeng, Y., Afjei, R., Robinson, E., Lau, K., Bermudez, A., Habte, F., Pitteri, S. J., Sinclair, R., Willmann, J. K., Massoud, T. F., Gambhir, S. S., & Paulmurugan, R. (2018). Tumor cell-derived extracellular vesicle-coated nanocarriers: an efficient theranostic platform for the cancer-specific delivery of Anti-miR-21 and imaging agents. *ACS Nano*, *12*(11), 10817–10832. [CrossRef] PMID: 30346694.

Jeyaram, A., & Jay, S. M. (2017). Preservation and storage stability of extracellular vesicles for therapeutic applications. *The Aaps Journal [Electronic Resource]*, *20*(1), 1.[CrossRef].

Jia, G., Han, Y., An, Y., Ding, Y., He, C., Wang, X., & Tang, Q. (2018). NRP-1 targeted and cargo-loaded exosomes facilitate simultaneous imaging and therapy of glioma in vitro and in vivo. *Biomaterials*, *178*, 302–316. [CrossRef] PMID: 29982104.

Jung, K. O., Jo, H., Yu, J. H., Gambhir, S. S., & Pratx, G. (2018). Development and MPI tracking of novel hypoxia-targeted theranostic exosomes. *Biomaterials*, *177*, 139–148. [CrossRef] PMID: 29890363.

Jung, K. O., Kim, Y.-H., Chung, S.-J., Lee, C.-H., Rhee, S., Pratx, G., Chung, J.-K., & Youn, H. (2020). Identification of lymphatic and hematogenous routes of rapidly labeled radioactive and fluorescent exosomes through highly sensitive multimodal imaging. *International Journal of Molecular Sciences*, *21*(21), 1-15. [CrossRef].

Karpman, D., Ståhl, A.-L., & Arvidsson, I. (2017). Extracellular vesicles in renal disease. *Nature Reviews Nephrology*, *13*(9), 545–562. [CrossRef] PMID: 28736435.

Kim, H. Y., Kim, T. J., Kang, L., Kim, Y.-J., Kang, M. K., Kim, J., Ryu, J. H., Hyeon, T., Yoon, B.-W., Ko, S.-B., & Kim, B.-S. (2020). Mesenchymal stem cell-derived magnetic extracellular nanovesicles for targeting and treatment of ischemic stroke. *Biomaterials*, *243*, 119942.[CrossRef] PMID: 32179302.

Kourembanas, S. (2015). Exosomes: Vehicles of intercellular signaling, biomarkers, and vectors of cell therapy. *Annual Review of Physiology*, *77*, 13–27. [CrossRef] PMID: 25293529.

Lai, C. P., Mardini, O., Ericsson, M., Prabhakar, S., Maguire, C. A., Chen, J. W., Tannous, B. A., & Breakefield, X. O. (2014). Dynamic biodistribution of extracellular vesicles in vivo using a multimodal imaging reporter. *ACS Nano*, *8*(1), 483–494. [CrossRef] PMID: 24383518.

Lai, R. C., Yeo, R. W. Y., Tan, K. H., & Lim, S. K. (2013). Exosomes for drug delivery - a novel application for the mesenchymal stem cell. *Biotechnology Advances*, *31*(5), 543–551. [CrossRef] PMID: 22959595.

Lara, P., Palma-Florez, S., Salas-Huenuleo, E., Polakovicova, I., Guerrero, S., Lobos-Gonzalez, L., Campos, A., Muñoz, L., Jorquera-Cordero, C., Varas-Godoy, M., Cancino, J., Arias, E., Villegas, J., Cruz, L. J., Albericio, F., Araya, E., Corvalan, A. H., Quest, A. F. G., & Kogan, M. J. (2020). Gold nanoparticle based double-labeling of melanoma extracellular vesicles to determine the specificity of uptake by cells and preferential accumulation in small metastatic lung tumors. *Journal of Nanobiotechnology*, *18*(1), 20.[CrossRef] PMID: 31973696.

Lassailly, F., Griessinger, E., & Bonnet, D. (2010). Microenvironmental contaminations" induced by fluorescent lipophilic dyes used for noninvasive in vitro and in vivo cell tracking. *Blood*, *115*(26), 5347–5354. [CrossRef] PMID: 20215639.

Lázaro-Ibáñez, E., Faruqu, F. N., Saleh, A. F., Silva, A. M., Tzu-Wen Wang, J., Rak, J., Al-Jamal, K. T., & Dekker, N. (2021). Selection of fluorescent, bioluminescent, and radioactive tracers to accurately reflect extracellular vesicle biodistribution in vivo. *ACS Nano*, *15*(2), 3212–3227. [CrossRef] PMID: 33470092.

Lee, J.-R., Park, B.-W., Kim, J., Choo, Y. W., H. Y., Yoon, J.-K., Kim, H., Hwang, J.-W., Kang, M., Kwon, S. P., Song, S. Y., Ko, I. O., Park, J.-A., Ban, K., Hyeon, T., Park, H.-J., & Kim, B.-S. (2020). Nanovesicles derived from iron oxide nanoparticles-incorporated mesenchymal stem cells for cardiac repair. *Science Advances*, *6*(18), eaaz0952.[CrossRef] PMID: 32494669.

Lehmann, T. P., Juzwa, W., Filipiak, K., Sujka-Kordowska, P., Zabel, M., Głowacki, J., Głowacki, M., & Jagodziński, P. P. (2016). Quantification of the asymmetric migration of the lipophilic dyes, DiO and DiD, in homotypic co-cultures of chondrosarcoma SW-1353 cells. *Molecular Medicine Reports*, *14*(5), 4529–4536. [CrossRef] PMID: 27748852.

Liu, T., Zhu, Y., Zhao, R., Wei, X., & Xin, X. (2020). Visualization of exosomes from mesenchymal stem cells in vivo by magnetic resonance imaging. *Magnetic Resonance Imaging*, *68*, 75–82. [CrossRef] PMID: 32027941.

Lu, C.-H., Chen, Y.-A., Ke, C.-C., Chiu, S.-J., Chen, C.-C., Hsieh, Y.-J., Yang, B.-H., & Liu, R.-S. (2021). preclinical characterization and in vivo imaging of (111)in-labeled mesenchymal stem cell-derived extracellular vesicles. *Molecular Imaging and Biology*, *23*(3), 361–371. [CrossRef] PMID: 33216285.

Nishida-Aoki, N., Tominaga, N., Kosaka, N., & Ochiya, T. (2020). Altered biodistribution of deglycosylated extracellular vesicles through enhanced cellular uptake. *Journal of extracellular vesicles*, *9*(1), 1713527.[CrossRef] PMID: 32082512.

Nuzhat, Z., Kinhal, V., Sharma, S., Rice, G. E., Joshi, V., & Salomon, C. (2017). Tumour-derived exosomes as a signature of pancreatic cancer - liquid biopsies as indicators of tumour progression. *Oncotarget*, *8*(10), 17279–17291. [CrossRef] PMID: 27999198.

Pan, S., Pei, L., Zhang, A., Zhang, Y., Zhang, C., Huang, M., Huang, Z., Liu, B., Wang, L., Ma, L., Zhang, Q., & Cui, D. (2020). Passion fruit-like exosome-PMA/Au-BSA@Ce6 nanovehicles for real-time fluorescence imaging and enhanced targeted photodynamic therapy with deep penetration and superior retention behavior in tumor. *Biomaterials*, *230*, 119606.[CrossRef] PMID: 31806405.

Perets, N., Betzer, O., Shapira, R., Brenstein, S., Angel, A., Sadan, T., Ashery, U., Popovtzer, R., & Offen, D. (2019). Golden exosomes selectively target brain pathologies in neurodegenerative and neurodevelopmental disorders. *Nano Letters*, *19*(6), 3422–3431. [CrossRef] PMID: 30761901.

Phinney, D. G., & Pittenger, M. F. (2017). Concise review: MSC-derived exosomes for cell-free therapy. *Stem Cells*, *35*(4), 851–858. [CrossRef] PMID: 28294454.

Prince, M. R., Zhang, H. L., Prowda, J. C., Grossman, M. E., & Silvers, D. N. (2009). Nephrogenic systemic fibrosis and its impact on abdominal imaging. *Radiographics*, *29*(6), 1565–1574. [CrossRef] PMID: 19959508.

Progatzky, F., Dallman, M. J., & Lo Celso, C. (2013). From seeing to believing: labeling strategies for in vivo cell-tracking experiments. *Interface Focus*, *3*(3), 20130001.[CrossRef] PMID: 23853708.

Pužar Dominkuš, P., Stenovec, M. ž., Sitar, S., Lasič, E., Zorec, R., Plemenitaš, A., Žagar, E., Kreft, M., & Lenassi, M. (2018). PKH26 labeling of extracellular vesicles: Characterization and cellular internalization of contaminating PKH26 nanoparticles. *Biochimica et Biophysica Acta Biomembranes*, *1860*(6), 1350–1361. [CrossRef] PMID: 29551275.

Qiu, B., Xie, D., Walczak, P., Li, X., Ruiz-Cabello, J., Minoshima, S., Bulte, J. W. M., & Yang, X. (2010). Magnetosonoporation: Instant magnetic labeling of stem cells. *Magnetic Resonance in Medicine*, *63*(6), 1437–1441. [CrossRef] PMID: 20512844.

Rajagopal, C., & Harikumar, K. B. (2018). The origin and functions of exosomes in cancer. *Frontiers in Oncology*, *8*, 66.[CrossRef] PMID: 29616188.

Rashid, M. H., Borin, T. F., Ara, R., Angara, K., Cai, J., Achyut, B. R., Liu, Y., & Arbab, A. S. (2019). Differential in vivo biodistribution of (131)I-labeled exosomes from diverse cellular origins and its implication for theranostic application. *Nanomedicine*, *21*, 102072.[CrossRef] PMID: 31376572.

Rayamajhi, S., Marasini, R., Nguyen, T. D. T., Plattner, B. L., Biller, D., & Aryal, S. (2020). Strategic reconstruction of macrophage-derived extracellular vesicles as a magnetic resonance imaging contrast agent. *Biomaterials Science*, *8*(10), 2887–2904. [CrossRef] PMID: 32300771.

Ruiz-Cabello, J., Barnett, B. P., Bottomley, P. A., & Bulte, J. W. M. (2011). Fluorine (19F) MRS and MRI in biomedicine. *Nmr in Biomedicine*, *24*(2), 114–129. [CrossRef] PMID: 20842758.

Russell, A. E., Sneider, A., Witwer, K. W., Bergese, P., Bhattacharyya, S. N., Cocks, A., Cocucci, E., Erdbrügger, U., Falcon-Perez, J. M., Freeman, D. W., Gallagher, T. M., Hu, S., Huang, Y., Jay, S. M., Kano, S.-I., Lavieu, G., Leszczynska, A., Llorente, A. M., Lu, Q., … Vader, P. (2019). Biological membranes in EV biogenesis, stability, uptake, and cargo transfer: An ISEV position paper arising from the ISEV membranes and EVs workshop. *Journal of Extracellular Vesicles*, *8*(1), 1684862.[CrossRef] PMID: 31762963.

Scrimgeour, L. A., Potz, B. A., Aboul Gheit, A., Shi, G., Stanley, M., Zhang, Z., Sodha, N. R., Ahsan, N., Abid, M. R, & Sellke, F. W. (2019). Extracellular vesicles promote arteriogenesis in chronically ischemic myocardium in the setting of metabolic syndrome. *Journal of the American Heart Association*, *8*(15), e012617.[CrossRef] PMID: 31354010.

Sharma, S., Zuñiga, F., Rice, G. E., Perrin, L. C., Hooper, J. D., & Salomon, C. (2017). Tumor-derived exosomes in ovarian cancer - liquid biopsies for early detection and real-time monitoring of cancer progression. *Oncotarget*, *8*(61), 104687–104703. [CrossRef] PMID: 29262670.

Shi, S., Li, T., Wen, X., Wu, S. Y., Xiong, C., Zhao, J., Lincha, V. R., Chow, D. S., Liu, Y., Sood, A. K., & Li, C. (2019). Copper-64 labeled PEGylated exosomes for in vivo positron emission tomography and enhanced tumor retention. *Bioconjugate Chemistry*, *30*(10), 2675–2683. [CrossRef] PMID: 31560538.

Simonsen, J. B. (2019). Pitfalls associated with lipophilic fluorophore staining of extracellular vesicles for uptake studies. *Journal of Extracellular Vesicles*, *8*(1), 1582237.[CrossRef] PMID: 30815239.

Son, S. H., Oh, J. M., Gangadaran, P., Ji, H. D., Lee, H. W., Rajendran, R. L., Baek, S. H., Gopal, A., Kalimuthu, S., Jeong, S. Y., Lee, S.-W., Lee, J., & Ahn, B.-C. (2020). White blood cell labeling with Technetium-99m ((99m)Tc) using red blood cell extracellular vesicles-mimetics. *Blood Cells, Molecules & Diseases*, *80*, 102375.[CrossRef] PMID: 31655394.

Song, S., Shim, M. K., Lim, S., Moon, Y., Yang, S., Kim, J., Hong, Y., Yoon, H. Y., Kim, I.-S., Hwang, K. Y., & Kim, K. (2020). In situ one-step fluorescence labeling strategy of exosomes via bioorthogonal click chemistry for real-time exosome tracking in vitro and in vivo. *Bioconjugate Chemistry*, *31*(5), 1562–1574. [CrossRef] PMID: 32369345.

Takahashi, Y., Nishikawa, M., Shinotsuka, H., Matsui, Y., Ohara, S., Imai, T., & Takakura, Y. (2013). Visualization and in vivo tracking of the exosomes of murine melanoma B16-BL6 cells in mice after intravenous injection. *Journal of Biotechnology*, *165*(2), 77–84. [CrossRef] PMID: 23562828.

Takov, K., Yellon, D. M., & Davidson, S. M. (2017). Confounding factors in vesicle uptake studies using fluorescent lipophilic membrane dyes. *Journal of Extracellular Vesicles*, 6(1), 1388731.[CrossRef] PMID: 29184625.

Tayyaba, Rehman, F. U., Shaikh, S., Tanziela, Semcheddine, F., Du, T., Jiang, H., & Wang, X. (2020). In situ self-assembled Ag-Fe3O4 nanoclusters in exosomes for cancer diagnosis. *Journal of Materials Chemistry. B*, 8(14), 2845–2855. [CrossRef] PMID: 32175535.

Théry, C., Witwer, K. W., Aikawa, E., Alcaraz, M. J., Anderson, J. D., Andriantsitohaina, R., Antoniou, A., Arab, T., Archer, F., Atkin-Smith, G. K., Ayre, D. C., Bach, J.-M., Bachurski, D., Baharvand, H., Balaj, L., Baldacchino, S., Bauer, N. N., Baxter, A. A., Bebawy, M., … Zuba-Surma, E. K. (2018). Minimal information for studies of extracellular vesicles 2018 (MISEV2018): A position statement of the International Society for Extracellular Vesicles and update of the MISEV2014 guidelines. *Journal of Extracellular Vesicles*, 7(1), 1535750.[CrossRef] PMID: 30637094.

Toribio, V., Morales, S., López-Martín, S., Cardeñes, B., Cabañas, C., & Yáñez-Mó, M. (2019). Development of a quantitative method to measure EV uptake. *Science Reports*, 9(1), 10522.[CrossRef] PMID: 31324885.

Van Dongen, H. M., Masoumi, N., Witwer, K. W., & Pegtel, D. M. (2016). Extracellular vesicles exploit viral entry routes for cargo delivery. *Microbiology and Molecular Biology Reviews*, 80(2), 369–386. [CrossRef] PMID: 26935137.

Varga, Z., Gyurkó, I., Pálóczi, K., Buzás, E. I., Horváth, I., Hegedűs, N., Máthé, D., & Szigeti, K. (2016). Radiolabeling of extracellular vesicles with (99m)Tc for quantitative in vivo imaging studies. *Cancer Biotherapy & Radiopharmaceuticals*, 31(5), 168–173. [CrossRef] PMID: 27310303.

Verweij, F. J., Balaj, L., Boulanger, C. M., Carter, D. R. F., Compeer, E. B., D'angelo, G., El Andaloussi, S., Goetz, J. G., Gross, J. C., Hyenne, V., Krämer-Albers, E.-M., Lai, C. P., Loyer, X., Marki, A., Momma, S., Nolte-'T Hoen, E. N. M., Pegtel, D. M., Peinado, H., Raposo, G., … Van Niel, G. (2021). The power of imaging to understand extracellular vesicle biology in vivo. *Nature Methods*, 18(9), 1013–1026. [CrossRef] PMID: 34446922.

Walczak, P., Kedziorek, D. A., Gilad, A. A., Lin, S., & Bulte, J. W. M. (2005). Instant MR labeling of stem cells using magnetoelectroporation. *Magnetic Resonance in Medicine*, 54(4), 769–774. [CrossRef] PMID: 16161115.

Walczak, P., Ruiz-Cabello, J., Kedziorek, D. A., Gilad, A. A., Lin, S., Barnett, B., Qin, L., Levitsky, H., & Bulte, J. W. M. (2006). Magnetoelectroporation: Improved labeling of neural stem cells and leukocytes for cellular magnetic resonance imaging using a single FDA-approved agent. *Nanomedicine*, 2(2), 89–94. [CrossRef] PMID: 17292120.

Wan, Z., Zhao, L., Lu, F., Gao, X., Dong, Y., Zhao, Y., Wei, M., Yang, G., Xing, C., & Liu, L. (2020). Mononuclear phagocyte system blockade improves therapeutic exosome delivery to the myocardium. *Theranostics*, 10(1), 218–230. [CrossRef] PMID: 31903116.

Wang, N., Chen, C., Yang, D., Liao, Q., Luo, H., Wang, X., Zhou, F., Yang, X., Yang, J., Zeng, C., & Wang, W. E. (2017). Mesenchymal stem cells-derived extracellular vesicles, via miR-210, improve infarcted cardiac function by promotion of angiogenesis. *Biochimica et Biophysica Acta - Molecular Basis of Disease*, 1863(8), 2085–2092. [CrossRef] PMID: 28249798.

Weinreb, J. C., & Abu-Alfa, A. K. (2009). Gadolinium-based contrast agents and nephrogenic systemic fibrosis: Why did it happen and what have we learned? *Journal of Magnetic Resonance Imaging*, 30(6), 1236–1239. [CrossRef] PMID: 19938035.

Willms, E., Cabañas, C., Mäger, I., Wood, M. J. A., & Vader, P. (2018). Extracellular vesicle heterogeneity: subpopulations, isolation techniques, and diverse functions in cancer progression. *Frontiers in immunology*, 9, 738.[CrossRef] PMID: 29760691.

Witwer, K. W., Van Balkom, B. W. M., Bruno, S., Choo, A., Dominici, M., Gimona, M., Hill, A. F., De Kleijn, D., Koh, M., Lai, R. C., Mitsialis, S. A., Ortiz, L. A., Rohde, E., Asada, T., Toh, W. S., Weiss, D. J., Zheng, L., Giebel, B., & Lim, S. K. (2019). Defining mesenchymal stromal cell (MSC)-derived small extracellular vesicles for therapeutic applications. *Journal of Extracellular Vesicles*, 8(1), 1609206.[CrossRef] PMID: 31069028.

Witwer, K. W., & Wolfram, J. (2021). Extracellular vesicles versus synthetic nanoparticles for drug delivery. *Nature Reviews Materials*, 6(2), 103–106. [CrossRef].

Wu, J.-Y., Ji, A.-L., Wang, Z.-X., Qiang, G.-H., Qu, Z., Wu, J.-H., & Jiang, C.-P. (2018). Exosome-Mimetic Nanovesicles from Hepatocytes promote hepatocyte proliferation in vitro and liver regeneration in vivo. *Science Reports*, 8(1), 2471.[CrossRef] PMID: 29410409.

Xie, D., Qiu, B., Walczak, P., Li, X., Ruiz-Cabello, J., Minoshima, S., Bulte, J. W. M., & Yang, X. (2010). Optimization of magnetosonoporation for stem cell labeling. *Nmr in Biomedicine*, 23(5), 480–484. [CrossRef] PMID: 20213856.

Xin, H., Li, Y., Cui, Y., Yang, J. J., Zhang, Z. G., & Chopp, M. (2013). Systemic administration of exosomes released from mesenchymal stromal cells promote functional recovery and neurovascular plasticity after stroke in rats. *Journal of Cerebral Blood Flow and Metabolism*, 33(11), 1711–1715. [CrossRef] PMID: 23963371.

Yu, X., He, L., Pentok, M., Yang, H., Yang, Y., Li, Z., He, N., Deng, Y., Li, S., Liu, T., Chen, X., & Luo, H. (2019). An aptamer-based new method for competitive fluorescence detection of exosomes. *Nanoscale*, 11(33), 15589–15595. [CrossRef] PMID: 31403149.

Zhang, K., Yu, L., Li, F.-R., Li, X., Wang, Z., Zou, X., Zhang, C., Lv, K., Zhou, B., Mitragotri, S., & Chen, M. (2020). Topical application of exosomes derived from human umbilical cord mesenchymal stem cells in combination with sponge spicules for treatment of photoaging. *International journal of nanomedicine*, 15, 2859–2872. [CrossRef] PMID: 32368058.